

1 **Direct measurement of N₂O₅ heterogeneous uptake coefficients on ambient**
2 **aerosols via an aerosol flow tube system: design, characterization and**
3 **performance**

4 Xiaorui Chen^{1,a}, Haichao Wang^{3,4*}, Tianyu Zhai¹, Chunmeng Li¹, Keding Lu^{1,2*}

5 ¹State Key Joint Laboratory of Environmental Simulation and Pollution Control, College of
6 Environmental Sciences and Engineering, Peking University, Beijing, China.

7 ²The State Environmental Protection Key Laboratory of Atmospheric Ozone Pollution Control,
8 College of Environmental Sciences and Engineering, Peking University, Beijing, China

9 ³School of Atmospheric Sciences, Sun Yat-sen University, Zhuhai, 519082, China

10 ⁴Guangdong Provincial Observation and Research Station for Climate Environment and Air
11 Quality Change in the Pearl River Estuary, Key Laboratory of Tropical Atmosphere-Ocean
12 System, Ministry of Education, Southern Marine Science and Engineering Guangdong
13 Laboratory (Zhuhai), Zhuhai, 519082, China

14 ^anow at: Department of Civil and Environmental Engineering, The Hong Kong Polytechnic
15 University, Hong Kong, China

16 *Correspondence to:* Haichao Wang (wanghch27@mail.sysu.edu.cn), Keding Lu
17 (k.lu@pku.edu.cn)

18

19 **Abstract.** An improved aerosol flow tube system coupled with detailed box model was
20 developed to measure N₂O₅ heterogeneous uptake coefficients ($\gamma(\text{N}_2\text{O}_5)$) on ambient aerosols
21 directly. This system features sequential measurements of N₂O₅ concentration at the both
22 entrance and exit of the flow tube to ensure an accurate retrieval of N₂O₅ loss in the flow tube.
23 Simulation and laboratory tests demonstrate that this flow tube system is able to overcome the
24 interference from side reactions led by varying reactants (e.g., NO₂, O₃ and NO) and improve
25 the robustness of results with the assistance of box model method. Factors related to $\gamma(\text{N}_2\text{O}_5)$
26 derivation were extensively characterized, including particle transmission efficiency, mean
27 residence time in the flow tube and wall loss coefficient of N₂O₅, for normal operating

28 condition. The measured $\gamma(\text{N}_2\text{O}_5)$ on $(\text{NH}_4)_2\text{SO}_4$ model aerosols were in good agreement with
29 literature values over a range of relative humidity (RH). The detection limit of $\gamma(\text{N}_2\text{O}_5)$ was
30 estimated to be 0.0016 at low aerosol surface concentration (Sa) condition of $200 \mu\text{m}^2 \text{cm}^{-3}$.
31 Given the instrument uncertainties and potential fluctuation of air mass between successive
32 sampling modes, we estimate the overall uncertainty of $\gamma(\text{N}_2\text{O}_5)$ that ranges from 16 to 43%
33 for different ambient conditions. This flow tube system was then successfully deployed for
34 field observations at an urban site of Beijing influenced by anthropogenic emissions. The
35 performance in field observation demonstrates that the current setup of this system is capable
36 of obtaining robust $\gamma(\text{N}_2\text{O}_5)$ amid the switch of air mass.

37 **1 Introduction**

38 Dinitrogen pentoxide (N_2O_5), forming from the reaction of nitrogen dioxide (NO_2) and nitrate
39 radical (NO_3), acts as an important reservoir of atmospheric nitrogen. The N_2O_5 can undergo
40 either thermal dissociation (back to NO_2 and NO_3 ; photolysis of NO_3 also generate NO_2) to
41 release NO_2 or hydrolysis (both homogeneous and heterogeneous) to remove nitrogen oxides
42 from the atmosphere (Brown and Stutz, 2012; Chang et al., 2011). Among the budgets of N_2O_5 ,
43 the uptake on aerosol particles is a highly efficient pathway to be responsible for production
44 of nitrate aerosol in some regions (Fu et al., 2020; Wang et al., 2019; Wang et al.,
45 2017c; Baasandorj et al., 2017; McDuffie et al., 2019; Prabhakar et al., 2017; Wang et al.,
46 2018a; Chen et al., 2020) and promote activation of chlorine via ClNO_2 formation (Bertram
47 and Thornton, 2009a; Osthoff et al., 2008; Tham et al., 2018; Thornton et al., 2010; Wang et al.,
48 2017f; Riedel et al., 2012a; Riedel et al., 2013; Gaston and Thornton, 2016; Mitroo et al., 2019).
49 The N_2O_5 uptake coefficient ($\gamma(\text{N}_2\text{O}_5)$) is critical in determining the uptake reaction rate of
50 N_2O_5 on aerosol in addition to aerosol surface area (Sa). It represents the fraction of collisions
51 between gaseous N_2O_5 molecules and particle surfaces that resulted in a loss of N_2O_5 . Model
52 simulation showed the variations in $\gamma(\text{N}_2\text{O}_5)$ can significantly influence the fate of NO_x , O_3
53 and OH radical in a regional (Li et al., 2016; Sarwar et al., 2012; Lowe et al., 2015) and global
54 scale (Dentener and Crutzen, 1993; Evans and Jacob, 2005; Macintyre and Evans, 2010; Murray

55 et al., 2021). However, ambient data of direct observation on $\gamma(\text{N}_2\text{O}_5)$ is still scarce. It is
56 thereby necessary to develop an accurate equipment or method to quantify this parameter on
57 ambient aerosols.

58 Extensive laboratory experiments have been conducted to derive the values of $\gamma(\text{N}_2\text{O}_5)$ on
59 aerosols and understand the mechanism of N_2O_5 uptake by various methods, including aerosol
60 flow reactor (Kane et al., 2001; Mozurkewich and Calvert, 1988; Hu and Abbatt,
61 1997; Thornton and Abbatt, 2005; Thornton et al., 2003; Tang et al., 2014; Bertram and Thornton,
62 2009a; Cosman et al., 2008; Escoreia et al., 2010; Gaston et al., 2014; Folkers et al., 2003),
63 droplet train reactor (Van Doren et al., 1990; Schweitzer et al., 1998), Knudsen flow reactor
64 (Karagulian et al., 2006) and smog chamber (Wahner et al., 1998; Wu et al., 2020). The $\gamma(\text{N}_2\text{O}_5)$
65 was found to be highly variable and dependent on particle chemical composition, acidity, size,
66 phase state and the presence of organic coating using these laboratory methods under
67 controllable conditions (Badger et al., 2006; Bertram et al., 2011; Fried et al., 1994; Griffiths et
68 al., 2009; Gross et al., 2009; Hallquist et al., 2000; McNeill et al., 2006; Mentel et al.,
69 1999; Riemer et al., 2003; Gaston and Thornton, 2016; Escoreia et al., 2010; Gaston et al.,
70 2014; Thornton et al., 2003). While laboratory results have contributed to recognize the
71 mechanism of N_2O_5 uptake and develop $\gamma(\text{N}_2\text{O}_5)$ parameterizations (Anttila et al.,
72 2006; Bertram and Thornton, 2009b; Davis et al., 2008; Griffiths et al., 2009; Riemer et al.,
73 2009), issues might emerge when quantitatively extended to ambient conditions due to the
74 discrepancy between laboratory conditions and real air mass. For example, much higher
75 reactant and particle concentration usually used in laboratory experiments might induce
76 surface saturation or secondary reactions in a short time period, which lead to the bias of
77 reaction rate used in ambient conditions (Thornton et al., 2003). In addition, the
78 physicochemical properties of ambient aerosol are much more complicated than the model
79 aerosol used in laboratory studies, which led to the laboratory results on model aerosols are
80 difficult to accurately represent what happens on the atmospheric aerosols (Royer et al.,
81 2021; Mitroo et al., 2019).

82 There have been several methods implemented for field campaigns to indirectly derive
83 $\gamma(\text{N}_2\text{O}_5)$, simply based on observation of ambient NO_3 , N_2O_5 , NO_2 , O_3 , ClNO_2 , pNO_3^- and

84 other auxiliary parameters without special equipment to capture the decay of N_2O_5 like
 85 laboratory ways. These include (1) the linear fit between N_2O_5 (NO_3) lifetime and the product
 86 of NO_2 and S_a concentration according to steady state equations (Brown et al., 2002; Brown et
 87 al., 2009; Brown et al., 2006; Platt et al., 1984; Wang et al., 2017b; Wang et al., 2017d; Tham et
 88 al., 2016; Wang et al., 2017f; Brown et al., 2016), (2) the analysis of production rates of
 89 products (pNO_3^- and $ClNO_2$) resulting from N_2O_5 uptake under a stable condition (Mielke et
 90 al., 2013; Phillips et al., 2016; Wang et al., 2018b) and (3) box model simulations with an
 91 iterative approach to reproduce the evolutions of NO_3 - N_2O_5 chemistry within each separate
 92 air mass after sunset (McDuffie et al., 2018; Wagner et al., 2013; Wang et al., 2020a; Yun et al.,
 93 2018). All these methods contain some specific assumptions and are only applicable in a few
 94 special cases.

95 To directly determine the $\gamma(N_2O_5)$ on ambient aerosols, Bertram et al. (2009a) firstly
 96 design an entrained aerosol flow reactor to adapt for low atmospheric S_a concentration with
 97 easy operation. By switching between filtered and bypass sampling mode, the N_2O_5
 98 concentration at the exit of flow tube can be measured in the presence and absence of aerosols,
 99 respectively. The pseudo-first-order rate coefficients for N_2O_5 loss on aerosols is thereby
 100 derived from the ratio of measured N_2O_5 concentration in these two modes within a duty cycle
 101 according to Eq. 1:

$$k_{aerosols} = -\frac{1}{\Delta t} \ln \frac{[N_2O_5]_{\Delta t}^{w/particles}}{[N_2O_5]_{\Delta t}^{wo/particles}} \quad \text{Eq. 1}$$

102 where the Δt is the mean residence time of the flow tube, and the $[N_2O_5]_{\Delta t}^{wo/particles}$ and
 103 $[N_2O_5]_{\Delta t}^{w/particles}$ are the measured N_2O_5 concentration at the exit of flow tube in filtered and
 104 bypass mode, respectively. Assuming the gas-phase diffusion effect is negligible for
 105 atmospheric particles and low reaction probability ($\gamma < 0.1$) (Fuchs and Sutugin, 1970), $\gamma(N_2O_5)$
 106 can then be calculated from Eq. 2:

$$\gamma(N_2O_5) = \frac{4 \times k_{aerosols}}{c \times S_a} \quad \text{Eq. 2}$$

107 This method was deployed to measure $\gamma(\text{N}_2\text{O}_5)$ on ambient particles during two field
 108 campaigns (Bertram et al., 2009b; Riedel et al., 2012b) and on aerosols generated in the
 109 laboratory (Ahern et al., 2018). While values of $\gamma(\text{N}_2\text{O}_5)$ were determined to be robust in
 110 laboratory experiments, most of data would be dropped under ambient conditions due to the
 111 variations of wall loss coefficients (dominated by RH), fresh NO emission, N_2O_5 regeneration
 112 and flow pattern inside the flow tube. Based on the above measurement system, Wang et al.
 113 (2018c) added NO_x , O_3 and Sa measurement on the exit of flow tube and introduce an iterative
 114 box model to minimize the potential influences from changing air mass and non-linear
 115 response of interference reactions. With the assumption of the equilibrium between NO_3 and
 116 N_2O_5 , the box model runs backward and forward iteratively to obtain the N_2O_5 loss rate
 117 constant in the absence ($k_{het}^{wo/particles}$) and presence ($k_{het}^{w/particles}$) of aerosols respectively.
 118 The difference between these two parameters can finally derived the $\gamma(\text{N}_2\text{O}_5)$ according to Eq.
 119 3, assuming the wall loss effect stays consistent.

$$\gamma(\text{N}_2\text{O}_5) = \frac{4(k_{het}^{w/particles} - k_{het}^{wo/particles})}{c \times S_a} \quad \text{Eq. 3}$$

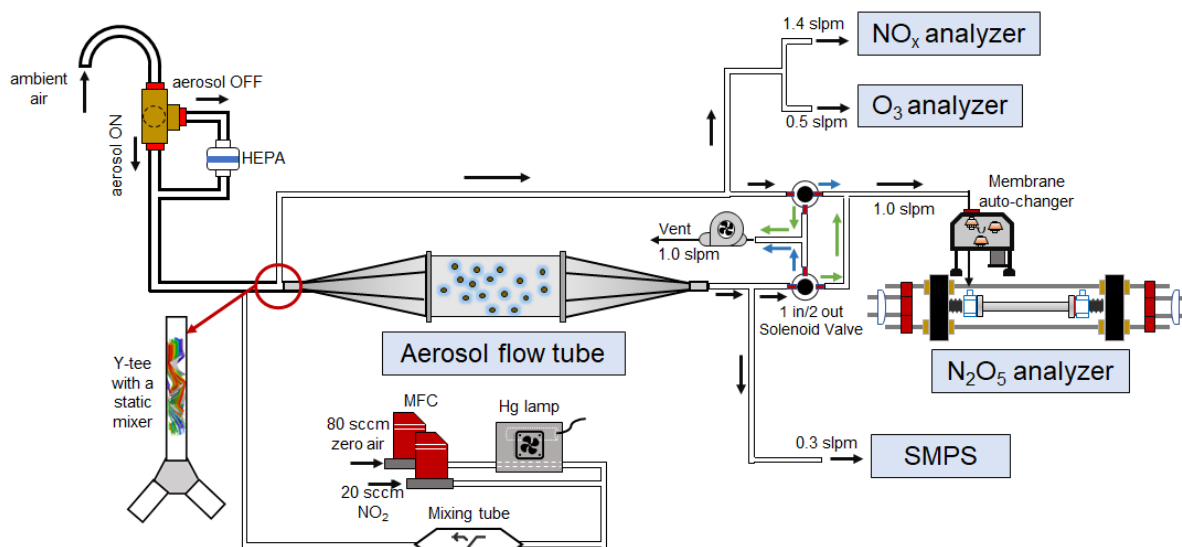
120 This iterative approach was demonstrated to be able to buffer against certain fluctuations of
 121 air mass and measure $\gamma(\text{N}_2\text{O}_5)$ in the polluted atmosphere (Yu et al., 2020b).

122 Until now, only few direct measurements of $\gamma(\text{N}_2\text{O}_5)$ on ambient aerosols have been
 123 conducted during field campaigns (Bertram et al., 2009b; Riedel et al., 2012b; Yu et al., 2020a).
 124 Even though combining with dataset from indirect approaches (e.g. steady state
 125 approximations), it is still challenging to characterize the temporal and spatial distributions of
 126 $\gamma(\text{N}_2\text{O}_5)$ on ambient aerosols. To better investigate the reactive uptake of N_2O_5 on aerosols in
 127 different environments, we develop an aerosol flow tube system with newly designed gas
 128 circuit and data acquisition procedures to quantify $\gamma(\text{N}_2\text{O}_5)$ on ambient aerosols. In the
 129 following sections, the setup of this system and laboratory characterizations for each part are
 130 described in details. Procedures of acquiring and processing data are compared to previous
 131 methods and discussed with potential uncertainties. Laboratory tests on model aerosols and
 132 field observations are presented to demonstrate its performance under varying ambient

133 conditions.

134 2 The aerosol flow tube system

135 A schematic of the aerosol flow tube system is shown in Figure 1. The ambient air enters
136 the system from the sampling manifold, mixes with gaseous N_2O_5 source in a Y-tee and flows
137 to aerosol flow tube and detection instruments, as indicated by arrows in the figure. The design
138 of sampling module and aerosol flow tube in this work follows previous work for measuring
139 $\gamma(N_2O_5)$ on ambient aerosols (e.g. Bertram et al., 2009). The major improvement of this system
140 from previous work are continuous monitor of NO_x and O_3 concentration before the inlet of
141 flow tube (after sampling air mixing with N_2O_5 source) and the sequential measurements of
142 N_2O_5 concentration both at the inlet and the exit of flow tube within a duty cycle. To achieve
143 the programmed cyclic measurement of these key parameters, we adopted a new design of Y-
144 tee with a static mixer inside and cyclic measurement setup.



145

146 **Figure 1.** Overall schematic of aerosol flow tube system. The arrows alongside the tube show
147 the flow directions. The black arrows indicate the flow directions consistent during the
148 measurements, green arrows indicate the flow directions active in measuring the exit N_2O_5
149 and blue arrows indicate the flow directions active in measuring the inlet N_2O_5 .

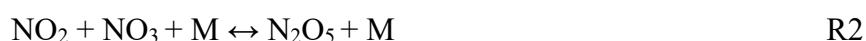
150 2.1 Sampling manifold

151 The sampling tube is made of a 50 cm long and half inch outside diameter (OD) aluminum
152 tubing, with a curve tip (10 cm radius of curvature) turning the inlet straight down in order to

153 avoid precipitation. The ambient air is then pass through a three-way stainless-base solenoid
154 ball valve, which is controlled by a time relay to either allow the air to flow directly into a
155 following Y-tee (filter bypass mode) or divert to a HEPA (high efficiency particulate air filter,
156 Whatman) to remove particles (filter inline mode). The HEPA can retain particles at a high
157 efficiency (>99.9%) with low pressure drop and RH difference between filter inline and bypass
158 mode.

159 **2.2 Gaseous N₂O₅ generation**

160 A home-made temperature-controlled gas generator is used to generate gaseous N₂O₅ in-situ
161 via the reaction of O₃ with NO₂ (R1) and the subsequent reaction of produced NO₃ with NO₂
162 (R2).



163 NO₂ is delivered from a compressed gas cylinder (20 ppmv in N₂ diluent gas, Jinghao Corp.).
164 O₃ is generated from the photolysis of O₂ in compressed ultra-pure synthetic zero air at 254
165 nm, using a commercial mercury lamp (UVP, the USA) fixed inside the generator. The
166 produced O₃ are then mixed with NO₂ in a Teflon chamber for about 2 min under the
167 temperature of 15 °C, stabilized by a Peltier cooler controlled by proportion integration
168 differentiation algorithm. A PFA tube with polyethylene foam was used to transmit the
169 synthesized N₂O₅ to sampling stream and minimize the influence of ambient temperature
170 variation on N₂O₅ level. The flow rate of NO₂ (20 sccm) and zero air (80 sccm) are controlled
171 by mass flow controller separately at a total of 100 sccm. By changing the flow rate ratio
172 between NO₂ and zero air, the generator can produce N₂O₅ concentration varying from 1 ppbv
173 to 6 ppbv (after dilution in zero air at sampling flow rate of 4.5 slpm). Under the typical
174 measurement condition, an excess of NO₂ concentration is applied to shift the equilibrium
175 towards N₂O₅ production (R2) and suppress the NO₃ concentration to less than 30 pptv, which
176 is expected to decrease the uncertainty of varying NO₃ reactivity (NO, VOCs and
177 heterogeneous loss). The resulted initial N₂O₅ concentration was 4.0 ppbv at the inlet of

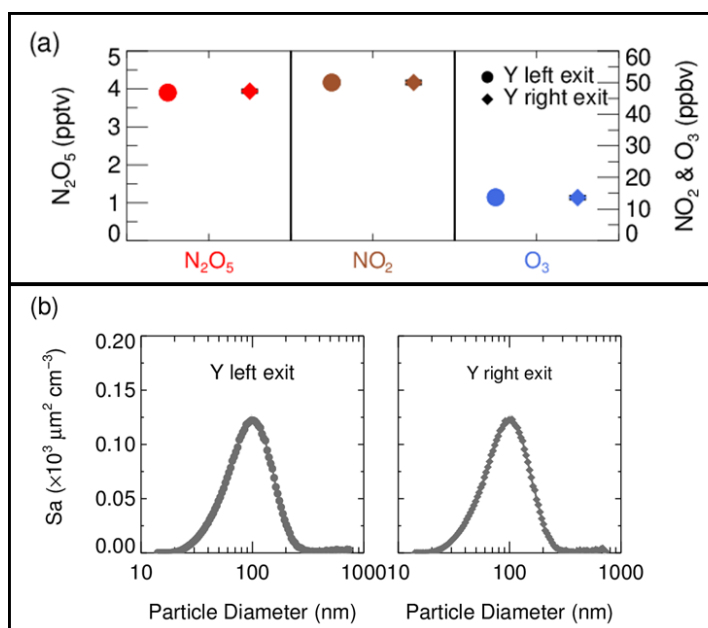
178 aerosol flow tube, together with around 50 ppbv of NO₂ and 15 ppbv of O₃. A stability test on
179 N₂O₅ source showed the variation was within 1% for a 24-h continuous operation, with
180 ambient temperature ranging from 0 to 15 °C.

181 **2.3 Aerosol flow tube**

182 Air flow enters and exits the flow tube via two identical conical diffuser caps at a diffuser
183 angle of 45°. A 35cm×14 cm inner diameter (ID) cylindrical tube is mounted in the middle
184 of two caps, flanged with screws and nitrile rubber O-rings. All sections of this aerosol flow
185 tube are made of stainless-steel with electro-polished and FEP-coated inside. The exterior of
186 the flow tube is insulated with aluminum coated polyethylene foam 3 cm thick to minimize
187 thermal eddies fluctuation of ambient temperature. The mechanic design of this flow tube
188 follows that used in Bertram et al. (2009), with different length and diffuser angles particularly
189 designed for our typical flow rate. Under the typical flow rate of 2.1 SLPM in the flow tube,
190 the axial velocity in the cylindrical tube section is 0.23 cm·s⁻¹ which produces a Reynolds
191 numbers (*Re*) of 22, well below the threshold of laminar flow (*Re*<2100).

192 In front of the flow tube, the synthesized N₂O₅ source is introduced perpendicular to
193 ambient air sampling stream and the mixture then enters a stainless-steel Y-tee for further
194 mixing. The inner surface of Y-tee is electro-polished and coated with SilcoNert 2000 (Silotek
195 Corp.), a technique commonly applied in semiconductor industry, to maintain the transmission
196 efficiency of particles and minimize the loss of N₂O₅ in the meantime. A 10 cm long stainless-
197 steel static mixer is mounted inside the Y-tee in order to swirl the flow and therefore facilitate
198 the mixing between sampling stream and N₂O₅ source in a relatively short distance. The
199 presence of static mixer in front of the inlet also help to improve the flow expansion after
200 entering the flow tube by minimizing recirculation zone, which decreases the wall loss of N₂O₅
201 and particles (Huang et al., 2017). After passing through the static mixer, the mixture of
202 ambient air and N₂O₅ source is split into two flows at the same flow rate, one of which
203 straightly enters the aerosol flow tube and the other one is diverted to measurements of NO_x,
204 O₃ and N₂O₅. We measured the concentrations of NO_x, O₃, N₂O₅ and Sa at the both exits of
205 Y-tee under typical flow rate for three repeated experiments (Figure 2). Almost the same

206 gaseous concentrations and particle distributions at both exits of Y-tee demonstrate that the
207 N_2O_5 source has been well mixed with the sampling flow.



208
209 **Figure 2.** (a) The concentration of N_2O_5 , NO_2 and O_3 in the mixture of N_2O_5 source and
210 sampling aerosols measured at each exit of Y-tee; (b) The size distribution of Sa concentration
211 in the mixture of N_2O_5 gas source and sampling aerosols measured at each exit of Y-tee.

212 2.4 Detection instruments

213 Instruments used in this system are listed in Table 1. A portable cavity-enhanced absorption
214 spectrometer (CEAS) is used to measure N_2O_5 concentration (Wang et al., 2017a) at both inlet
215 and exit of the aerosol flow tube by automatically switching the flow directions (see details in
216 section 2.5). Briefly, the N_2O_5 is thermally decomposed to NO_3 by heating up to $130^\circ C$ and
217 then quantified according to the extinction coefficient caused by NO_3 absorption in the
218 wavelength window from 640 to 680 nm. A Teflon polytetrafluoroethylene (PTFE) membrane
219 is placed in front of the CEAS to remove particles, which will be replaced with a new one
220 every two hours by a self-designed membrane auto-changer. Laboratory tests have been
221 conducted to quantify the transmission efficiency of N_2O_5 over the membrane ($92\pm 3\%$),
222 sampling tube of CEAS (99.7%) and the inside of CEAS (93.6%). The use of a filter upstream
223 of the CEAS and the procedures of membrane changing have been successfully applied in
224 many field campaigns to measure ambient N_2O_5 (Brown et al., 2016; Kennedy et al.,

225 2011;Wang et al., 2017a;Wang et al., 2017b;Wang et al., 2018a). The loss of N₂O₅ on
 226 membrane filter, sampling tube and the detection chamber inside the CEAS were corrected
 227 according to transmission efficiency. The detection limit of N₂O₅ was determined to be 2.7
 228 pptv (1 σ , 60 s) with the measurement uncertainty of 19%. The CEAS has been successfully
 229 applied to measure ambient N₂O₅ concentration in several field campaigns and laboratory
 230 studies (Chen et al., 2020;Wang et al., 2020a;Wang et al., 2017b;Wang et al., 2020b;Wang et
 231 al., 2018b;Wang et al., 2022).

232 **Table 1.** Performance of related instruments incorporated in the flow tube system.

Parameter	Technique	Time resolution	Detection Limit(1 σ)	Accuracy
NO	Chemiluminescence ^a	1 min	200 pptv	$\pm 10\%$
NO ₂	Chemiluminescence	1 min	300 pptv	$\pm 10\%$
O ₃	UV photometry	1 min	500 pptv	$\pm 5\%$
VOCs	GC-MS/FID ^b	60 min	20-300 pptv	$\pm 15\%$
N ₂ O ₅	CEAS	1 min	2.7 pptv	$\pm 19\%$
Sa	SMPS	5 min	-	$\pm 10\%$
RH&T	Sensor	1 min	-	$\pm 0.1\% \& \pm 0.1K$

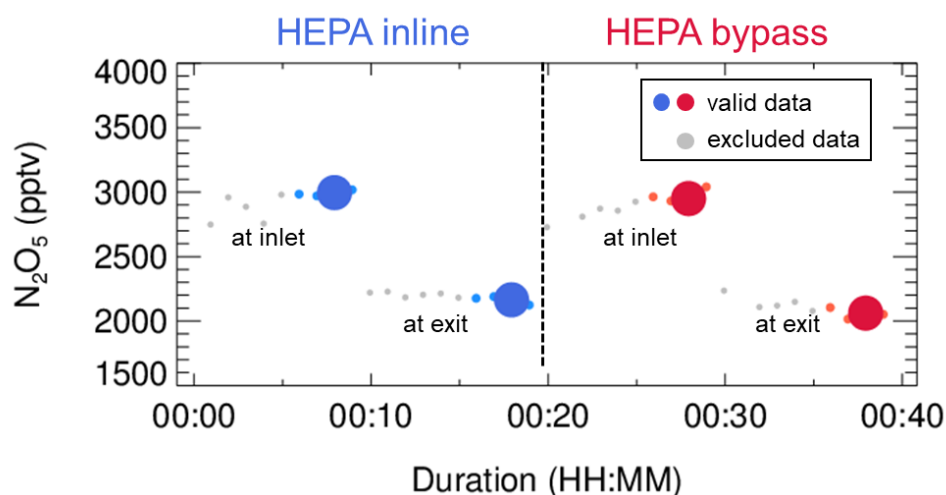
233 ^a Photolytic conversion to NO through blue light before detection; ^b Gas chromatography
 234 equipped with a mass spectrometer and a flame ionization detector;

235 At the inlet of flow tube, NO_x concentration is measured via chemiluminescence method
 236 equipped with a blue-light photolytic converter (Thermo, Model 42i) and O₃ concentration is
 237 also measured via chemiluminescence method by adding excessive NO (Teledyne API, Model
 238 T265). Both NO_x and O₃ concentration are averaged to 1 min time-resolution. The size
 239 distribution of particle number density is measured at the exit of flow tube using a scanning
 240 mobility particle sizer (SMPS, TSI 3776), which determines the total Sa concentration
 241 covering the range from 13 to 730 nm. Particles larger than this range usually contributed less
 242 than 5% of total Sa according to our previous field measurements (Chen et al., 2020) and it is
 243 included in the uncertainty analysis (see section 5). A cycle of size scanning is set to around 5
 244 min and the derived Sa concentration is then interpolated into 1 min for further calculation.
 245 Aerosols pass through a Nafion tubing (MD-700) before entering into SMPS to reduce RH to
 246 less than 30%. The dry-state Sa is therefore corrected to wet-state at the RH inside the flow

247 tube for particle hygroscopicity. The growth factor, $f(\text{RH})=1+8.77\times(\text{RH}/100)^{9.74}$, used for
248 correction is valid only when RH is within the range from 30 to 90% (Liu et al., 2013). The
249 RH and temperature of flow are continuously measured both before entering and after leaving
250 the flow tube by commercial sensors (Rotronic, Model HC2A-S). The averages of the values
251 obtained at both locations are used to represent the RH and temperature inside the flow tube.
252 In addition, ambient volatile organic compounds (VOCs) are measured in-situ alongside the
253 aerosol flow tube system using an online gas chromatograph mass spectrometer coupled with
254 a flame ionization detector (GCMS-FID) to derive the NO_3 reactivity to VOCs ($k_{\text{NO}_3\text{-VOCs}}$) in
255 the flow tube.

256 **2.5 Procedures of data acquisition**

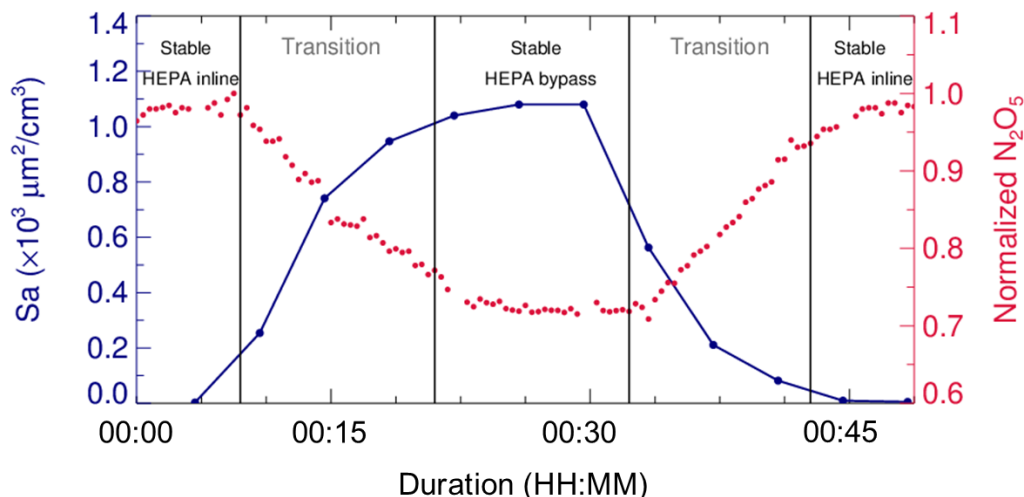
257 The N_2O_5 concentration is acquired at both inlet and exit of the flow tube within a duty cycle
258 via a CEAS instrument, which is different from that only at the exit of the flow tube in previous
259 studies (Bertram et al., 2009a; Wang et al., 2018c). Each duty cycle consists of once HEPA
260 inline mode for measuring k_{wall} of N_2O_5 and once HEPA bypass mode for retrieving the N_2O_5
261 loss on aerosols. The procedure that measuring N_2O_5 at the inlet of flow tube first and then at
262 the exit is executed within each mode. An exemplary case obtained during a field campaign is
263 shown in Figure 3 to explain this procedure. Within the mode of HEPA inline, N_2O_5 data is
264 firstly acquired at the inlet of the flow tube and then switch to the exit of the flow tube. The
265 $k_{\text{het}}^{\text{wo/particles}}$, which is the k_{wall} of N_2O_5 , can be derived from a box model constrained by these
266 N_2O_5 data (see section 3 for the model description and data processing). The same procedures
267 are executed in the mode of HEPA bypass, except the $\gamma(\text{N}_2\text{O}_5)$ is derived according to Eq 2.
268 Two three-way valves controlled by a time relay were implemented to realize this procedure
269 in order to avoid the changes of flow condition in the flow tube that could have been caused.
270 As indicated in Figure 1, the blue arrows show the flow directions when measuring the N_2O_5
271 concentration at the inlet of flow tube, while the green arrows shows that for the exit of flow
272 tube. It should be noted that the concentration of NO_x and O_3 are always acquired at the inlet
273 of the flow tube and the Sa concentration always at the exit of the flow tube during the
274 operation.



275
 276 **Figure 3.** An exemplary case of measured N_2O_5 concentration within a duty cycle. This case
 277 was observed on the night of 13 December 2020, with average ambient S_a of $320 \mu\text{m}^2 \text{cm}^{-3}$.
 278 The derived k_{wall} of N_2O_5 and $\gamma(\text{N}_2\text{O}_5)$ were 0.0023 s^{-1} and 0.035 , respectively. The blue dots
 279 indicate N_2O_5 concentration measured under the mode of HEPA inline either at the inlet or
 280 exit of the flow tube (denoted as texts); the respective averages (blue dots of larger size) are
 281 used for deriving k_{wall} (blue square). The red dots indicate N_2O_5 concentration measured under
 282 the mode of HEPA bypass either at the inlet or exit of the flow tube; the respective averages
 283 (red dots of larger size) are used for deriving the overall rate constant of N_2O_5 loss on the wall
 284 and aerosols. The data points in gray are excluded from calculation due to unstable conditions
 285 in the flow tube.

286 In addition, laboratory tests were conducted to determine a suited duration for each duty
 287 cycle. During a duty cycle, the duration for each mode should last long enough to develop a
 288 stable flow condition for particles or empty particles, while a much longer duration could
 289 decrease the measurement time-resolution and leads to large uncertainty due to the fluctuations
 290 within a long time period. We measured S_a and N_2O_5 concentration continuously at the exit of
 291 flow tube when sampling $(\text{NH}_4)_2\text{SO}_4$ aerosols. As shown in Figure 4, it took about 15 minutes
 292 for particles to rise to a stable level from none or to decrease from a certain level to none, when
 293 our system underwent mode switches. The periodical variation of N_2O_5 concentration was
 294 consistent with particles. The residence time distribution (RTD) profiles (see in section 4.2)
 295 also demonstrated that a pulse injection of NO_2 requires 10~15 minutes to be fully drained out
 296 of the flow tube, which to some extent supports the 15-minute time required for complete
 297 mixing of N_2O_5 . As a result, a typical duration of duty cycle is composed of 40 minutes with

298 20 minutes for each mode, which is similar to that in Bertram et al. (2009). The N₂O₅
 299 measurement at the exit of the flow tube in the last 5 minutes of each mode is able to represent
 300 valid decays of N₂O₅ under this mode and satisfy the requirements of further data processing.



301
 302 **Figure 4.** Variations of Sa and N₂O₅ concentration (normalized to peak values) measured at
 303 the exit of flow tube when switching the sampling mode. The phases of species concentrations
 304 in the flow tube approaching stable after a mode switch are denoted as the transition phases.

305 **3 Box model for determination of loss rate coefficients of N₂O₅**

306 **3.1 Method description**

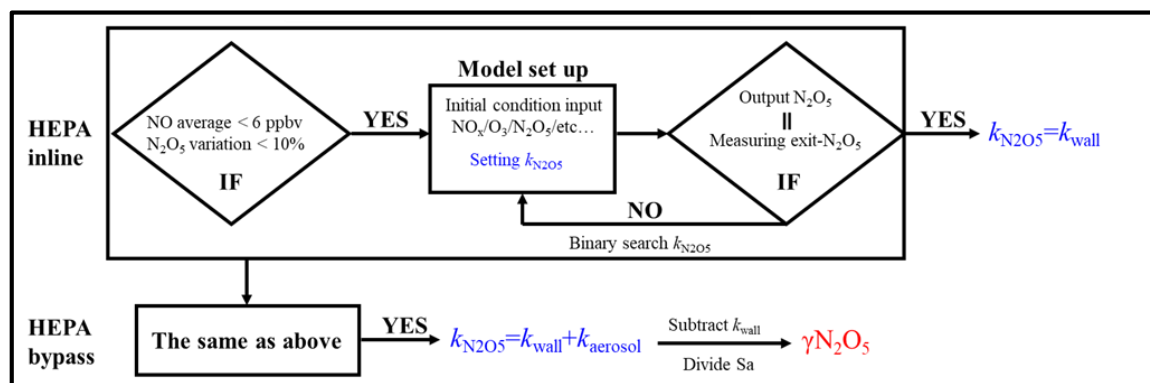
307 Large uncertainties were found in retrieving $\gamma(\text{N}_2\text{O}_5)$ on ambient particles according to Eq. 1
 308 in a previous flow tube study (Bertram et al., 2009a), due to the dependence of homogeneous
 309 reaction rates on sampling modes and the atmospheric variations of parameters related to NO₃-
 310 N₂O₅ chemistry (e.g. NO, NO₂, O₃, VOCs, and RH). To minimize these influences, a time-
 311 dependent box model constrained by the measurements of N₂O₅ concentration and other
 312 auxiliary parameters is applied to calculate loss rate coefficients of N₂O₅ under the mode of
 313 HEPA inline and bypass, respectively. The model is able to simulate the reactions related to
 314 budgets of NO₃-N₂O₅ chemistry in a dark condition, including R1, R2 and the follows:



315 The rate constants for reactions R1 to R3 are referenced to IUPAC database. The reaction of
316 VOCs and NO₃ is treated as pseudo-first-order with a rate constant of $k_{\text{NO}_3\text{-VOCs}}$, which is the
317 sum of rate constants for reactions of NO₃ with each VOCs scaled by the concentration of
318 VOCs measured by GC-FID. In this work, there are 30 kinds of measured VOCs having known
319 reaction rate constants with NO₃ included in the model (Table A1). Due to low time-resolution
320 of VOCs measurements (1 h), the $k_{\text{NO}_3\text{-VOCs}}$ is kept constant for each derivation of $\gamma(\text{N}_2\text{O}_5)$.
321 The suppressed NO₃ concentration is expected to attenuate the influence resulted from the
322 uncertainty of $k_{\text{NO}_3\text{-VOCs}}$ (see discussion in section 5). The reaction R5 represents the loss of
323 N₂O₅ only on the wall in the mode of HEPA inline or on the both wall and particles in the
324 mode of HEPA bypass. The rate constant of R5 is also treated as pseudo-first-order and it is
325 adjustable among different runs.

326 The same procedures of data screening and model operation are applied to both sampling
327 and bypass modes, as shown in Figure 5. For example, in the mode of HEPA inline, the average
328 of NO concentration less than 6 ppbv and the variation of N₂O₅ measured at the inlet of flow
329 tube less than 10% should be validated prior to the following model operation. Under typical
330 concentration of N₂O₅ source we used in this flow tube system, the exit concentration of N₂O₅
331 is detected to be under triple detection limit with initial NO large than 6 ppbv according to our
332 laboratory tests. In ambient condition, high level of NO is usually also accompanied by rapid
333 variation due to fresh emission, which disturbs the decay of N₂O₅ in the flow tube and leads
334 to large uncertainty in deriving its loss rate coefficient. Excluding the cases that N₂O₅
335 measured at the inlet of flow tube varies exceeding 10% can further minimize the uncertainty
336 of N₂O₅ loss rate coefficient resulted from rapid change of NO₃ reactants (NO, VOCs). If the
337 measured data within the duration of a sampling mode satisfies the criteria for data screening
338 described above, the model can therefore simulate the reactions starting from the entrance of
339 flow tube and lasting for 156 s (mean residence time) based on these data. The initial
340 concentrations of $[\text{NO}]_{t=0}$, $[\text{NO}_2]_{t=0}$, $[\text{O}_3]_{t=0}$ and $[\text{N}_2\text{O}_5]_{t=0}$ are the averages of last-5-min values
341 measured at the inlet of flow tube. The RH and temperature are constrained by the mean values

342 during this sampling mode. By tuning the loss rate coefficient of N_2O_5 ($k_{N_2O_5}$) in the way of
 343 binary search, we optimized an appropriate $k_{N_2O_5}$ to ensure that the N_2O_5 concentration output
 344 from the simulation is consistent with last-5-min average of N_2O_5 concentration measured at
 345 the exit of flow tube within 1 pptv. As a result, this derived $k_{N_2O_5}$ (aka. $k_{het}^{wo/particles}$) is
 346 expected to be the k_{wall} of N_2O_5 . The same procedures above are then applied to the data
 347 obtained in the mode of HEPA bypass, except that the derived $k_{N_2O_5}$ (aka. $k_{het}^{w/particles}$)
 348 contains the loss rate coefficients of N_2O_5 on the both wall and particles. It should be noted
 349 that the above calculation for obtained data is only valid under the variation of RH less than
 350 2% within a duty cycle and the k_{wall} of N_2O_5 can then be reasonably assumed to be constant
 351 between two successive sampling modes. Therefore, the $\gamma(N_2O_5)$ can be retrieved by the Eq 3,
 352 where the last-5-min averages of Sa concentration in the mode of HEPA bypass is used.



353

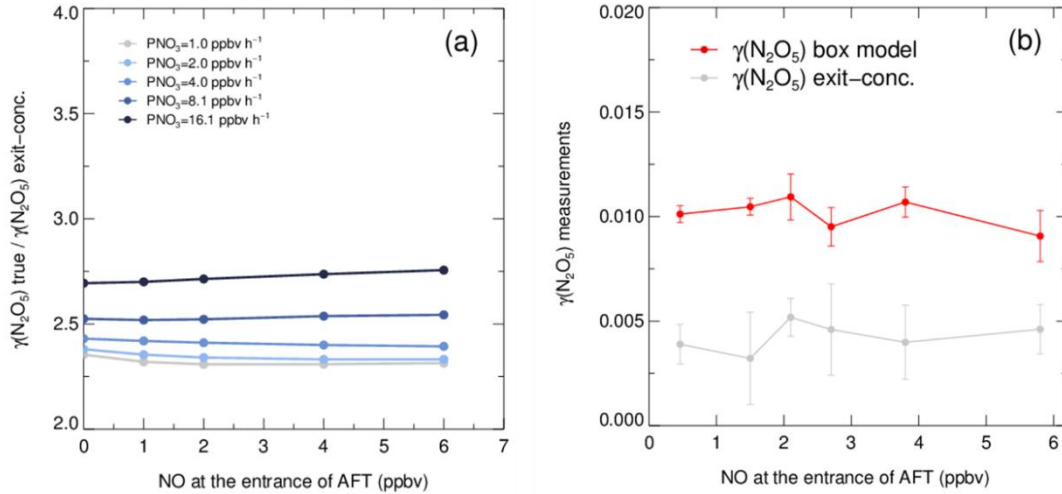
354 **Figure 5.** Flow diagram of $\gamma(N_2O_5)$ derivation through box model method.

355 **3.2 Evaluation of the box model method**

356 The box model method is introduced to our flow tube system to overcome the influence from
 357 homogeneous reactions and variations of air mass on $\gamma(N_2O_5)$ retrieval. A series of scenarios
 358 were provided to evaluate the performance of box model method by both simulations and
 359 laboratory experiments. We allow NO, NO₂ and O₃ in the mixture of sampling air at the
 360 entrance of the flow tube to vary in a reasonable range, in order to develop the scenarios of
 361 different gradients of NO concentration and NO₃ production rates (PNO₃). The levels of PNO₃
 362 was adjusted by NO₂ and O₃ concentrations (O₃ ranging from 10 to 80 ppbv and NO₂ ranging
 363 from 50 to 160 ppbv) under the temperature of 283 K and RH of 30%. In simulation studies,

364 the exit concentration of N_2O_5 would be obtained from the simulated N_2O_5 evolutions with
365 and without particles in the flow tube. To corroborate the results estimated by simulations,
366 laboratory tests were performed on $(NH_4)_2SO_4$ aerosols to measure the exit concentration of
367 N_2O_5 under varying NO concentration. The $\gamma(N_2O_5)$ on particles are then calculated according
368 to Eq 1&2 or by box model method described above.

369 As shown in Figure 6(a), the exit concentration method ($\gamma(N_2O_5)$ exit-conc., derived
370 directly by Eqs. 1-2) underestimates $\gamma(N_2O_5)$ and the extent of underestimation increases with
371 PNO_3 levels in simulation tests. Similarly, the exit concentration method underestimates
372 $\gamma(N_2O_5)$ by 50 to 60% with PNO_3 of 1.0 ppbv h^{-1} in the laboratory tests (Figure 6(b)). Noted
373 that the $\gamma(N_2O_5)$ was determined to be at around 0.01 by box model method over the NO range
374 from 0 to 6 ppbv, which agrees well with previous laboratory observation of $\gamma(N_2O_5)$ on
375 $(NH_4)_2SO_4$ aerosols within uncertainty (Badger et al., 2006; Hallquist et al., 2003; Kane et al.,
376 2001). The cause of $\gamma(N_2O_5)$ exit-conc. underestimation is mainly due to the in situ N_2O_5
377 production in the flow tube. With a continuous production of NO_3 via the reaction of NO_2 and
378 O_3 and rapid heterogeneous loss of N_2O_5 in the flow tube, the equilibrium between NO_3 and
379 N_2O_5 always shifts to the production of N_2O_5 , and masking the actual amount of N_2O_5 removal.
380 In the mode of HEPA bypass, the N_2O_5 consumes faster than the other mode due to the addition
381 of particles, which further facilitates the N_2O_5 formation through the equilibrium. Previous
382 studies also found similar impacts from N_2O_5 production on retrieving $\gamma(N_2O_5)$ in the aerosol
383 flow tube (Bertram et al., 2009a; Wang et al., 2018c). However, the discrepancy of $\gamma(N_2O_5)$
384 derived by two methods is much less dependent on the NO concentration, at least within the
385 prescribed range, due to relatively small ratio of NO_3/N_2O_5 in the N_2O_5 source. The absence
386 of dependence between NO concentration and $\gamma(N_2O_5)$ also indicates that this aerosol flow
387 tube system can buffer against NO within the range from 0 to 6 ppbv under typical operating
388 condition. However, this is not always the case when there is a rapid fluctuation of NO in a
389 real atmosphere, which might lead to intractable uncertainty and is therefore excluded from
390 further analysis according to the criteria of data screening.



391

392 **Figure 6.** Simulated and laboratory tests on performance of box model method and exit
 393 concentration method for $\gamma(\text{N}_2\text{O}_5)$ derivation. (a) The ratios of given $\gamma(\text{N}_2\text{O}_5)$ ($\gamma(\text{N}_2\text{O}_5)$ true)
 394 over exit concentration derived $\gamma(\text{N}_2\text{O}_5)$ ($\gamma(\text{N}_2\text{O}_5)$ exit-conc.) determined from simulated
 395 scenarios. The $\gamma(\text{N}_2\text{O}_5)$ derived by box model method is exactly the same as $\gamma(\text{N}_2\text{O}_5)$ true. The
 396 ratios vary with NO concentration and the lines are color coded by PNO_3 values. Both NO
 397 concentration and PNO_3 represent the values at the entrance of aerosol flow tube. (b) $\gamma(\text{N}_2\text{O}_5)$
 398 measurements on lab-generated $(\text{NH}_4)_2\text{SO}_4$ aerosols under different gradients of NO with
 399 constant RH of 50% and PNO_3 typically generated from our N_2O_5 source. The red line shows
 400 the $\gamma(\text{N}_2\text{O}_5)$ derived by box model method and gray line shows the $\gamma(\text{N}_2\text{O}_5)$ derived by exit
 401 concentration method. The NO concentrations are measured at the entrance of aerosol flow
 402 tube.

403 In comparison to the work by Bertram et al. (2009) and Wang et al. (2018), the
 404 combination of above box model method and the improved flow tube system in this study has
 405 progress in the following aspects. First, the dynamic quantification of k_{wall} of N_2O_5 within each
 406 duty cycle based on the constraint of sequentially measured N_2O_5 source is helpful to provide
 407 accurate data for both k_{wall} and $\gamma(\text{N}_2\text{O}_5)$ retrieval. The k_{wall} in ambient conditions could deviate
 408 from the results from laboratory tests (Figure B1) due to temperature variation and particles
 409 adsorption, which leads to large uncertainty when calculating $\gamma(\text{N}_2\text{O}_5)$ without the frequent
 410 determination of k_{wall} . While the k_{wall} was also determined frequently in the flow tube of Wang
 411 et al. (2018), the N_2O_5 source they used for k_{wall} and $\gamma(\text{N}_2\text{O}_5)$ retrieval is an assumed stable
 412 value instead of an observed one. Second, the concentrations of initial NO, NO_2 , O_3 and N_2O_5
 413 at the entrance of the flow tube, and exit N_2O_5 are obtained through programed cyclic

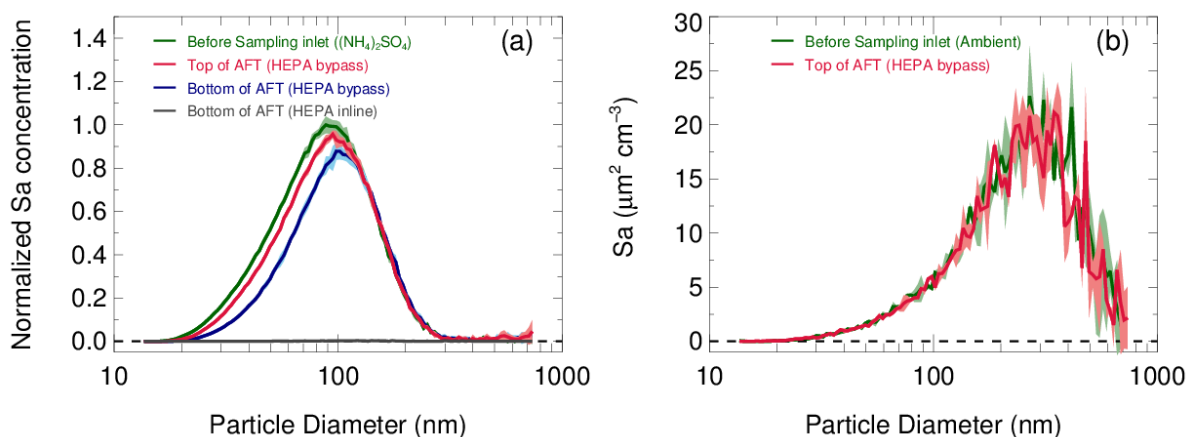
414 measurements in this work, which can reduce the uncertainties by adding the model constraints.
415 It is different from the iterative box model used in Wang et al. (2018) as we enable a
416 straightforward simulation of $\text{NO}_3\text{-N}_2\text{O}_5$ chemistry occurring in the flow tube, instead of
417 estimating the initial NO_2 and O_3 with assumed NO profile and stable N_2O_5 source based on
418 backward simulations. In ambient conditions, the initial N_2O_5 concentration can be largely
419 influenced by air mass conditions (especially NO concentration and temperature). Figure B2(a)
420 presents box whisker plot of N_2O_5 and NO concentration at the flow tube entrance during a
421 field campaign, which shows a much larger variation of N_2O_5 than in lab condition ($<1\%$). As
422 a result, the box model would underestimate $\gamma(\text{N}_2\text{O}_5)$ by using a fixed initial N_2O_5
423 concentration under certain circumstances (Figure B2(b)). Third, we simulate $\text{NO}_3\text{-N}_2\text{O}_5$
424 relationship via specific reactions rather than approximating it in equilibrium and introducing
425 the equilibrium coefficient (K_{eq}) into calculation. Calculating NO_3 or N_2O_5 concentration by
426 K_{eq} could induce large bias (up to 90%) under the high aerosol loading and low temperature
427 (Chen et al., 2021).

428 **4 Laboratory characterizations**

429 **4.1 Particle transmission efficiency**

430 The transmission efficiency of particles in the sampling module and flow tube are estimated
431 respectively in Figure 7. In the laboratory, pure ammonia nitrate ($(\text{NH}_4)_2\text{SO}_4$) aerosols were
432 generated from an atomizer loading with 0.1 M $(\text{NH}_4)_2\text{SO}_4$ solution. The RH and concentration
433 of produced aerosols flow was conditioned in a glass bottle (~ 2 L) by introducing a humidified
434 dilution flow of ultrahigh-purity N_2 . As a result, aerosols in different concentrations
435 ($1000\sim 4500 \mu\text{m}^2 \text{cm}^{-3}$) and under a range of RH (20~70%) were applied to test the
436 transmission efficiency. Figure 7(a) shows the loss of total Sa concentration in the sampling
437 module and flow tube are $8\pm 1\%$ and $10\pm 2\%$ on average, respectively. We found that the
438 fraction of particles loss is mainly caused by particles smaller than 100 nm. This is most likely
439 due to the turbulence generated by static mixer and the recirculation in the flow tube. Large
440 particles are prone to stay within the main flow direction, whereas small particles readily

441 adsorb on the walls by the entrainment of turbulence or recirculation. In addition, the particles
 442 distribution measured at the exit of flow tube with HEPA inline (gray line in Figure 7(a))
 443 demonstrated its capability of removing almost all particles (>99.5%) at the typical flow rate.
 444 The same transmission efficiency was also found on ambient aerosols (Figure 7(b)) as that on
 445 laboratory-generated aerosols. The results we obtained from above particle transmission
 446 experiments are similar to the findings of Bertram et al. (2009).



447
 448 **Figure 7.** (a) Particles transmission determined by sampling laboratory-generated $(\text{NH}_4)_2\text{SO}_4$
 449 aerosols. Aerosols at different concentrations and RH levels are used in experiments and the
 450 size distribution of Sa concentration are normalized to the peak values. The normalized size
 451 distribution of Sa concentration measured before sampling inlet (green line), at the inlet of
 452 flow tube with HEPA bypass (red line) and at the bottom of flow tube with HEPA bypass
 453 (blue line) are shown respectively. Under the mode of HEPA inline, the Sa concentration was
 454 almost zero at the bottom of flow tube (gray line). The shadows indicate the standard
 455 deviations of the normalized Sa concentration for all experiments. (b) Particles transmission
 456 determined by sampling ambient particles.

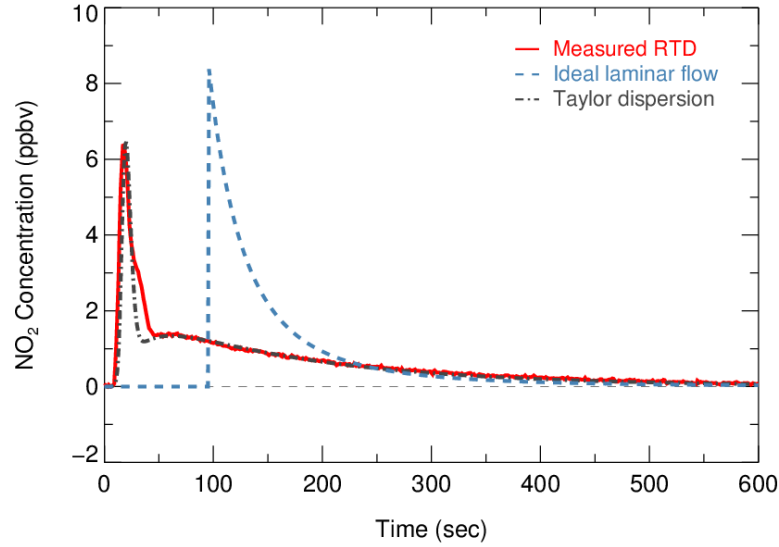
457 4.2 Residence time in the flow tube

458 The method of residence time distribution (RTD) was applied to estimate the average reaction
 459 time of the gas species in the flow tube (residence time). In comparison to ideal plug flow, the
 460 RTD method can better describe actual behavior of the flow in practice and determine the
 461 mean residence time more accurately (Danckwerts, 1953). Several studies have also used this
 462 RTD method to determine the residence time in the flow tube (Huang et al., 2017; Wang et al.,
 463 2018c; Lambe et al., 2011).

464 The RTD profiles were obtained by introducing a 2 s pulse of NO₂ gas diluted in N₂ into
465 the flow tube under RH less than 1%. NO₂ is relatively inert against the flow tube wall coated
466 with FEP and was measured at the exit of the flow tube by a CEAS (Li et al., 2021) at high
467 time-resolution (2 Hz). A three-way solenoid valve combined with a time relay was
468 implemented to control the pulse in order to avoid the disturbance on flow condition from the
469 injection. Experiments were performed under typical operation. The mean residence time (t_{ave})
470 can be derived from the each RTD profile according to Eq. 4,

$$t_{ave} = \frac{\sum_{i=0} C_i \times t_i}{\sum_{i=0} C_i}, \quad \text{Eq. 4}$$

471 where the C_i is the concentration of NO₂ recorded at the time step t_i . From the RTD profiles
472 of NO₂ injection experiments in Figure 8, the determined t_{ave} was 156 ± 3 s. This value is 19%
473 less than the space time (τ_{space} , flow tube volume divided by operation flow rate, 192.6 s). It
474 has also been found that the assumption of ideal plug flow overestimated the residence time
475 in previous flow tube experiments (Lambe et al., 2011; Huang et al., 2017; Wang et al., 2018c),
476 which could lead to underestimation of the derived $k_{N_2O_5}$. The residence time of current set up
477 is designed for investigating $\gamma(N_2O_5)$ in typical episode days with medium to high aerosol
478 loadings (the Sa concentration usually larger than $500 \text{ um}^2 \text{ cm}^{-3}$) in polluted regions. As shown
479 in Section 5, the detection limit of this system is 6.4×10^{-4} with Sa of $500 \text{ um}^2 \text{ cm}^{-3}$, which is
480 well below the most of previous ambient $\gamma(N_2O_5)$ results ranging from 1×10^{-3} to >0.1 in
481 polluted regions of China (Wang et al., 2020a; Wang et al., 2017d; Wang et al., 2017e; Xia et al.,
482 2019). The residence time determined in this work is also slightly higher than 149 s that
483 reported in a previous work focusing on investigating $\gamma(N_2O_5)$ in polluted regions (Wang et al.,
484 2018c). In addition, the residence time for this flow tube can be extended to over 300 s to
485 satisfy the $\gamma(N_2O_5)$ measurement requirements under low Sa by reducing the flow rate of air
486 passing through, which is controlled by an extra pump.



487

488 **Figure 8.** Residence time distribution derived by sampling NO₂ gas. Red solid line indicates
 489 the measured RTD profiles. The calculated RTD of ideal laminar flow (without dispersions)
 490 and the Taylor dispersion model fitted to measurements are shown as blue dash line and dot-
 491 dash line, respectively.

492 Two theoretical RTDs were calculated, namely ideal laminar flow and Taylor diffusion,
 493 besides the measured RTD, intending to reflect the fluid field inside the flow tube. The ideal
 494 laminar flow describes the flow without dispersion. The velocity profile of ideal laminar flow
 495 is parabolic, with the fluid in the center of the tube moving the fastest. According to the
 496 following Eq. 5, the RTD of ideal laminar flow is scaled by the integrated concentration of
 497 NO₂ and presented as the blue dash line in Figure 8.

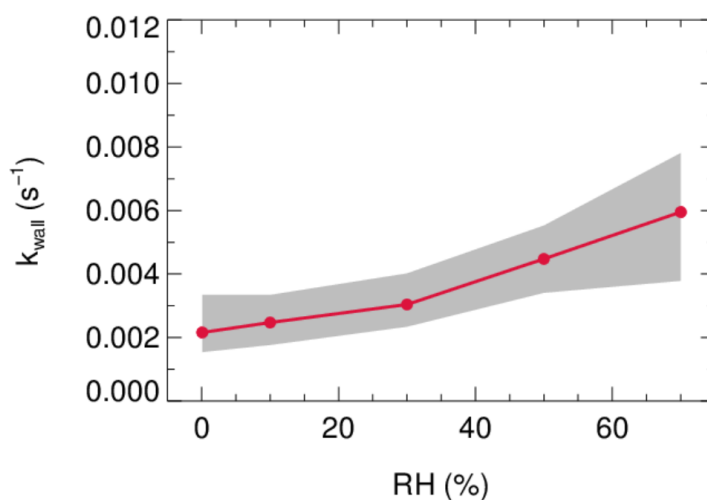
$$\begin{cases} 0, & t < 0.5\tau_{space} \\ \frac{\tau_{space}^2}{2t^3}, & t \geq 0.5\tau_{space} \end{cases}, \quad \text{Eq. 5}$$

498 While the determined *Re* is well within the laminar flow threshold, the measured RTD occurs
 499 earlier than theoretical laminar flow condition and exhibits a broaden distribution. The
 500 discrepancy between them indicates that the dispersions or potential secondary flows could
 501 dominate the flow regime. Instead, an improved Taylor dispersion model (shown as the gray
 502 dot-dash line in Figure 8) is able to reproduce the measured RTD, which was previously
 503 implemented in the characterization of photooxidation flow reactors (Lambe et al., 2011). Two
 504 flow patterns with distinct effective diffusivities (0.02 and 0.51 derived from best fit) were
 505 considered in this dispersion model. An implication from the characteristics of the model is

506 that two flow components consist of the flow regime: a direct flow path through the flow tube
 507 with less diffusion and a secondary flow path representing the recirculation in the dead zone
 508 that induced by temperature gradient and significant diffusions (Huang et al., 2017).

509 4.3 N₂O₅ wall loss

510 Laboratory tests were conducted to quantify the k_{wall} of N₂O₅ under different levels of RH with
 511 HEPA inline. As shown in Figure 9, the k_{wall} of N₂O₅ gradually increase from 0.002 s⁻¹ in a dry
 512 condition to 0.006 s⁻¹ when RH is 70%. The level of k_{wall} is less than the result of Wang et al.
 513 (2018c) but higher than Bertram et al. (2009a) as indicated in Table 2. In addition, the flow
 514 tube was rinsed with deionized water every week during the field campaigns to remove the
 515 build-up of particles, which might increase the hygroscopicity of the internal surface and thus
 516 the k_{wall} of N₂O₅ in a wet condition. Uncertainty in $\gamma(\text{N}_2\text{O}_5)$ derivation resulted from the
 517 variation of k_{wall} related to RH is discussed in section 5.



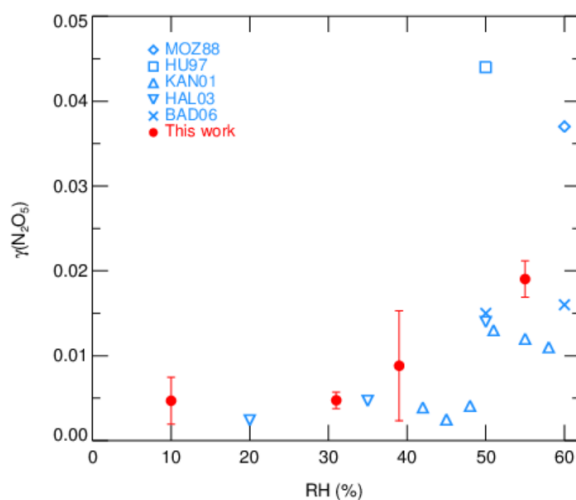
518
 519 **Figure 9.** The dependence of pseudo-first-order wall loss coefficient (k_{wall}) of N₂O₅ in the
 520 FEP-coated aerosol flow tube.

521 **Table 2.** Summary of the k_{wall} of N₂O₅ for the existing aerosol flow tube deployed in field
 522 campaigns.

RH range	k_{wall} range ($\times 10^{-3}$ s ⁻¹)	References
5~50%	0.5~3	Bertram et al., 2009
20~70%	4~9	Wang et al., 2018
0~70%	2~6	This work

523 4.4 Demonstration of $\gamma(\text{N}_2\text{O}_5)$ measurements on model particles

524 $\gamma(\text{N}_2\text{O}_5)$ measurements by current aerosol flow tube system equipped with box model method
525 were performed on lab-generated $(\text{NH}_4)_2\text{SO}_4$ aerosols over a range of RH. The system was
526 operated at room temperature of 295K with N_2O_5 concentration of 4.0 ppbv at the entrance of
527 flow tube. We conditioned the RH of generated aerosols by introducing dry N_2 gas dilution,
528 which could decrease the RH level down to 10~55%, starting from over 95% where $(\text{NH}_4)_2\text{SO}_4$
529 aerosols are expected to be in aqueous state. The resulting Sa concentrations of aerosols were
530 around $600 \mu\text{m}^2 \cdot \text{cm}^{-3}$. As shown in Figure 10, the observed $\gamma(\text{N}_2\text{O}_5)$ values were below 0.01
531 when RH was within 40% and significantly rose up to 0.02 with higher RH. The dependence
532 of $\gamma(\text{N}_2\text{O}_5)$ on RH and the exact values are well consistent with previous laboratory results on
533 $(\text{NH}_4)_2\text{SO}_4$ aerosols (Badger et al., 2006; Hallquist et al., 2003; Hu and Abbatt, 1997; Kane et
534 al., 2001; Mozurkewich and Calvert, 1988), which shows that the setup of our instrument has
535 good practicability. A large standard deviation of $\gamma(\text{N}_2\text{O}_5)$ found at RH of 39% is possibly due
536 to the unstable phase transition of $(\text{NH}_4)_2\text{SO}_4$ particles, as its efflorescence RH is reportedly
537 from 35 to 48% (Martin, 2000).



538

539 **Figure 10.** The dependence of $\gamma(\text{N}_2\text{O}_5)$ on RH for laboratory-generated $(\text{NH}_4)_2\text{SO}_4$ aerosols.
540 The red points with standard deviations represent the values measured by current aerosol flow
541 tube system in this work. Previously reported values are indicated in blue marks.

542 **5 Uncertainty analysis and detection limit**

543 The uncertainty of $\gamma(\text{N}_2\text{O}_5)$ is in relevance to the measurement uncertainties of each instrument
544 and rapid fluctuations of various parameters. As outlined before, the 5-min averages of N_2O_5
545 concentration measured at the inlet and exit of the flow tube were used for calculating $\gamma(\text{N}_2\text{O}_5)$
546 via the box model method. The potential variations within these selected time periods would
547 therefore lead to relative errors. For example, the variations of N_2O_5 concentration is resulted
548 majorly from the rapid changes of ambient NO and less from variations of VOCs, NO_2 , O_3 as
549 well as N_2O_5 gas source itself (1% in 24 hours). A cutoff of 10% for N_2O_5 variation was
550 implemented to filter out the air mass that was too unstable for valid analysis, according to our
551 prescribed criteria of data screening. It consequently leads to 10% uncertainty in the average
552 of N_2O_5 and can translate into a deviation of 2% in $\gamma(\text{N}_2\text{O}_5)$ with the $\gamma(\text{N}_2\text{O}_5)$ at 0.02, Sa at
553 $800 \mu\text{m}^2 \cdot \text{cm}^{-3}$ and other parameters (shown in Table 3) representing the typical inlet values
554 measured during the field campaign (described in section 6). Similarly, cases that over 2%
555 variation in RH exists between the HEPA inline and bypass mode are excluded from analysis,
556 owing to its significant influence on k_{wall} of N_2O_5 in the flow tube. By assuming a consistent
557 k_{wall} in successive sampling modes, the potential variations in RH could lead to uncertainty in
558 $\gamma(\text{N}_2\text{O}_5)$ from $\pm 8 \times 10^{-4}$ at RH of 20% to $\pm 2 \times 10^{-3}$ at RH of 70%, respectively, with the Sa at
559 $800 \mu\text{m}^2 \text{ cm}^{-3}$. In addition, the $k_{\text{NO}_3\text{-VOCs}}$ is treated as constant in a duty cycle due to the limit
560 of time resolution of VOCs measurements. A variation of $\pm 0.01 \text{ s}^{-1}$ in $k_{\text{NO}_3\text{-VOCs}}$ only induces
561 less than $\pm 1\%$ uncertainty in $\gamma(\text{N}_2\text{O}_5)$ for more than 95% cases obtained during the field
562 campaign. All the impacts from inherent instruments uncertainties and variations of different
563 parameters are thereby considered in Monte Carlo simulations to assess the overall uncertainty
564 of $\gamma(\text{N}_2\text{O}_5)$. The basic simulation is initialized with the typical conditions measured at the inlet
565 of the flow tube during the field campaign and repeatedly performs the procedures of
566 determining $\gamma(\text{N}_2\text{O}_5)$ via the box model method 1000 times. In each run, all parameters were
567 allowed to vary independently within a prescribed range. The basic simulation condition and
568 variation range are presented in Table 3.

569 **Table 3.** Parameters involved in the Monte Carlo simulations.

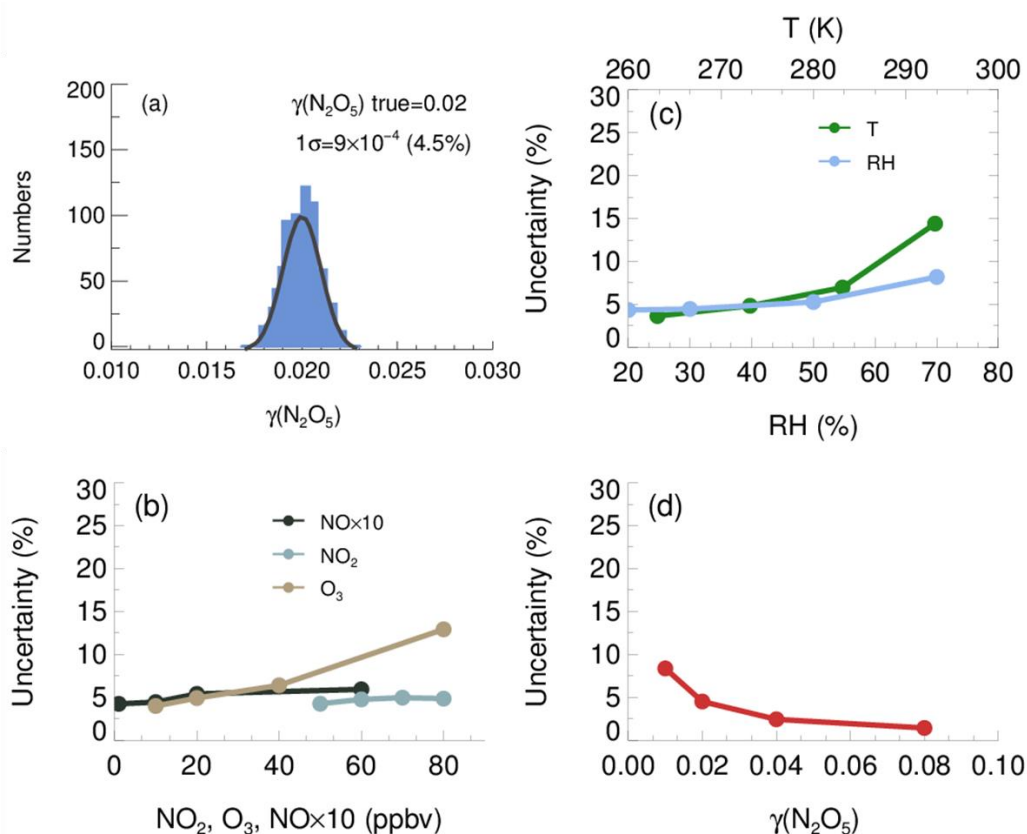
Parameters	Value ^a	Variation range ^b
NO	1 ppbv	±10%
NO ₂	70 ppbv	±10%
O ₃	10 ppbv	±5%
Inlet N ₂ O ₅	4 ppbv	±19%
Exit N ₂ O ₅ ^c	2.2 ppbv	±19%
Temperature	273 K	±0.1 K
RH ^d	30 %	±1%
$k_{\text{NO}_3\text{-VOCs}}$	0.01 s ⁻¹	±0.01 s ⁻¹

570 ^a Values used for initializing Monte Carlo simulations in a basic scenario; ^b Ranges within
571 which each parameter can vary independently; ^c Determined from the case that $\gamma(\text{N}_2\text{O}_5)$ is at
572 0.02, Sa is at 800 $\mu\text{m}^2\cdot\text{cm}^{-3}$ and other parameters are shown in this table; ^d The RH and its
573 variation can be transformed into values in k_{wall} of N₂O₅ via the fitting function derived from
574 Figure 9.

575 The resulting $\gamma(\text{N}_2\text{O}_5)$ values from Monte Carlo simulations under the basic scenario are
576 shown as frequency distributions in Figure 11(a). This distribution can be fitted by a Gaussian
577 function and the standard deviation (1σ) of Gaussian distribution is regarded as the overall
578 uncertainty of $\gamma(\text{N}_2\text{O}_5)$, which is $\pm 9 \times 10^{-4}$ (4.5% relative to true $\gamma(\text{N}_2\text{O}_5)$). The uncertainty of
579 Sa measurements and unmeasured particles larger than 730 nm (usually less than 5% of total
580 Sa) would together introduce an extra 16% uncertainty to $\gamma(\text{N}_2\text{O}_5)$.

581 We further found that the uncertainty of $\gamma(\text{N}_2\text{O}_5)$ could be sensitive to the measurement
582 conditions. With higher O₃, potential variations of NO and $k_{\text{NO}_3\text{-VOCs}}$ will induce larger
583 uncertainty of $\gamma(\text{N}_2\text{O}_5)$ (Figure 11(b)), as it enhances the abundance of NO₃ and N₂O₅. In
584 comparison, the low O₃ in the basic scenario suppressed the side formation of NO₃ in the flow
585 tube, limiting the aggravation of $\gamma(\text{N}_2\text{O}_5)$ uncertainty from the increase of NO and NO₂. The
586 $\gamma(\text{N}_2\text{O}_5)$ uncertainty is also positive correlated with RH and T. As is discussed before, the k_{wall}
587 of N₂O₅ increases with RH level, which can amplify the potential bias of k_{wall} at a higher RH
588 level. The equilibrium between NO₃ and N₂O₅ shifts towards the decomposition of N₂O₅ at
589 higher T, leading to larger uncertainty of $\gamma(\text{N}_2\text{O}_5)$ caused by potential variations of NO and

590 $k_{\text{NO}_3\text{-VOCs}}$. The overall uncertainty of $\gamma(\text{N}_2\text{O}_5)$ therefore rises to 8.2% at the RH of 70% and to
 591 14.4% at the temperature of 293K (Figure 11(c)), with NO, NO₂, O₃, $\gamma(\text{N}_2\text{O}_5)$ and Sa keeping
 592 the same as the basic scenario. In addition, Monte Carlo simulations were also performed for
 593 different $\gamma(\text{N}_2\text{O}_5)$ values ranging from 0.01 to 0.08. The uncertainty of $\gamma(\text{N}_2\text{O}_5)$ clearly
 594 decreased with the $\gamma(\text{N}_2\text{O}_5)$ (Figure 11(d)). A lower $\gamma(\text{N}_2\text{O}_5)$ weaken the impacts N₂O₅ uptakes
 595 has on the budgets of NO₃ and N₂O₅, which causes the $\gamma(\text{N}_2\text{O}_5)$ derivation to be more
 596 susceptible to uncertainties of other parameters and then increases the uncertainty of $\gamma(\text{N}_2\text{O}_5)$.

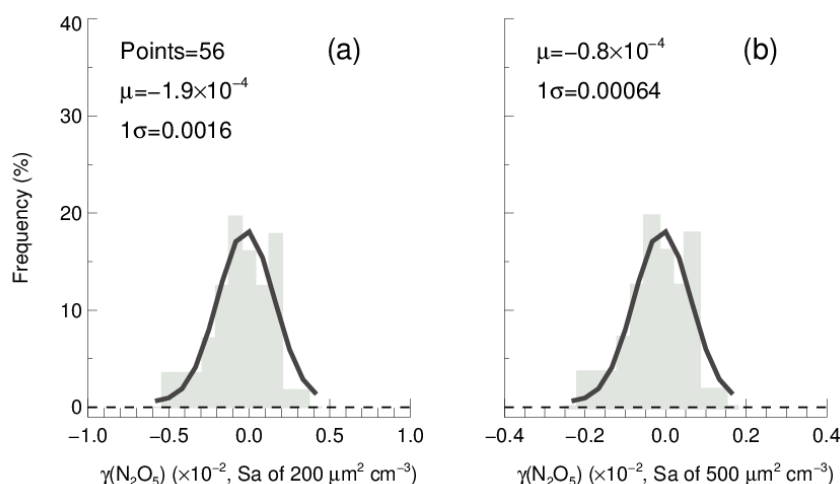


597
 598 **Figure 11.** The uncertainty of $\gamma(\text{N}_2\text{O}_5)$ determined from the Monte Carlo simulations. (a)
 599 Histogram distribution of $\gamma(\text{N}_2\text{O}_5)$ generated from a Monte Carlo simulation (1000 single runs)
 600 in the basic scenario (shown as Table 3), where the overall uncertainty of $\gamma(\text{N}_2\text{O}_5)$ was
 601 determined to be $\pm 9 \times 10^{-4}$; (b) dependence of the uncertainty of $\gamma(\text{N}_2\text{O}_5)$ on NO, NO₂ as well
 602 as O₃; (c) dependence of the uncertainty of $\gamma(\text{N}_2\text{O}_5)$ on RH and T; (d) dependence of the
 603 $\gamma(\text{N}_2\text{O}_5)$ uncertainty on $\gamma(\text{N}_2\text{O}_5)$ level.

604 In addition, the mean residence time used in the box model method could bias the retrieved
 605 $\gamma(\text{N}_2\text{O}_5)$ due to the non-normal distribution of residence time with a discernable tail. The
 606 reactants entrained by those slower streamlines close to the wall will take much longer time to

607 reach the exit of the flow tube than that by the centerline. In order to evaluate the uncertainty
608 caused by the distribution of residence time, we first performed simulations of N_2O_5 decay in
609 the flow tube under the basic scenarios and calculate the exit N_2O_5 concentration according to
610 the probability distribution function derived from RTD profile. Then the $\gamma(\text{N}_2\text{O}_5)$ can be
611 retrieved from the box model method running for the duration of mean residence time,
612 constrained by this calculated exit N_2O_5 concentration. The result shows that the use of mean
613 residence time produces 32% underestimation of $\gamma(\text{N}_2\text{O}_5)$ in the basic scenario. The extent of
614 underestimation is most sensitive to the level of $\gamma(\text{N}_2\text{O}_5)$ and RH. In short, when taking all the
615 factors and their corresponding varying ranges discussed above into consideration, the overall
616 uncertainty of $\gamma(\text{N}_2\text{O}_5)$ determined from Monte Carlo simulations is in the range of 16-43%.
617 To directly compare with previous studies, at 0.03 $\gamma(\text{N}_2\text{O}_5)$ with $1000 \mu\text{m}^2 \text{cm}^{-3} \text{Sa}$, the
618 uncertainty is calculated to be 19% which is lower than that ~24% in Bertram et al (2009) and
619 that ranging 37%~40% in Wang et al (2018).

620 In order to determine the detection limit of the current aerosol tube system, the continuous
621 blank measurements in zero air were performed with settled operation procedures. Within per
622 duty cycle (40 minutes), one k_{wall} of N_2O_5 and one $\gamma(\text{N}_2\text{O}_5)$ can be derived in pair. In total, we
623 obtained 56 sets of result. The detection limit of $k_{\text{N}_2\text{O}_5}$ on aerosols is $2.1 \times 10^{-5} \text{s}^{-1}$, derived from
624 1σ of the Gaussian function fitted to this distribution. It is equivalent to 0.0016 for the detection
625 limit of $\gamma(\text{N}_2\text{O}_5)$ with a low Sa condition of $200 \mu\text{m}^2 \text{cm}^{-3}$ (Figure 12(a)), and 0.00064 for the
626 detection limit of $\gamma(\text{N}_2\text{O}_5)$ with a moderate Sa condition of $500 \mu\text{m}^2 \text{cm}^{-3}$ (Figure 12(b)). This
627 result indicates that the flow tube system has capability of quantifying $\gamma(\text{N}_2\text{O}_5)$ for most cases
628 even under a low aerosol-loading environment.



629

630 **Figure 12.** The $\gamma(\text{N}_2\text{O}_5)$ derived from blank measurements in histogram distribution plot. The
 631 $\gamma(\text{N}_2\text{O}_5)$ was calculated from $k_{\text{N}_2\text{O}_5}$ by Eq 2 with Sa of (a) $200 \mu\text{m}^2 \text{cm}^{-3}$ and (b) $500 \mu\text{m}^2 \text{cm}^{-3}$,
 632 respectively, under the temperature of 293K. The Gaussian function is fitted to the distribution
 633 and plotted in black line. The 1σ from Gaussian fit is regarded as the detection limit.

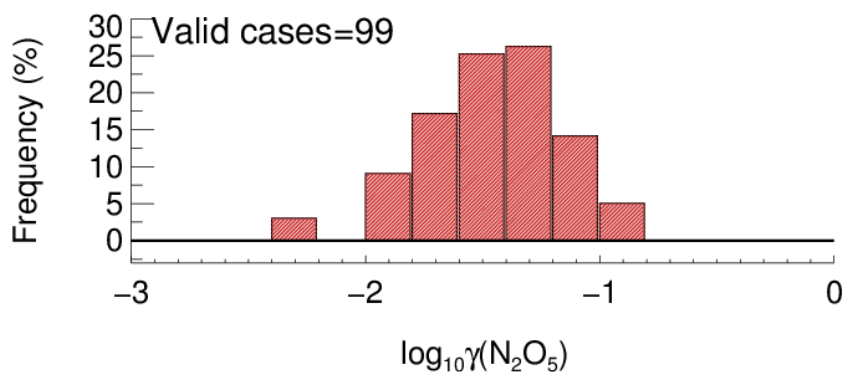
634 **6 Performance in the field campaign**

635 The aerosol flow tube system was successfully deployed to measure $\gamma(\text{N}_2\text{O}_5)$ on ambient
 636 aerosols in Beijing lasting for 20 days during the December of 2020. The sampling site was at
 637 the campus of Peking University, which is located in the city center of Beijing surrounded by
 638 major roads with heavy traffic. Therefore, this site represents an area with large amount of
 639 fresh emission of NOx and other anthropogenic sources. The system was mounted in the top
 640 floor of a building, about 15 m height above the ground. The sampling manifold was placed
 641 in open air and the ambient aerosols could directly enter the inlet of the manifold without
 642 additional sampling tubes. During the period of measurement, the averages of ambient
 643 temperature, RH, NO, NO₂, O₃ and Sa were $273 \pm 3 \text{ K}$, $25 \pm 12 \%$, $23 \pm 36 \text{ ppbv}$, $23 \pm 12 \text{ ppbv}$,
 644 $16 \pm 15 \text{ ppbv}$ and $409 \pm 249 \mu\text{m}^2 \text{cm}^{-3}$, respectively. The NO and Sa levels could vary by 2
 645 orders of magnitude due to the periodical switch between clean air mass from the north and
 646 pollutants accumulated by local emission.

647 A total of 99 valid $\gamma(\text{N}_2\text{O}_5)$ values were determined from the measurements based on the
 648 criteria of data screening described in section 3.1. We found that $\gamma(\text{N}_2\text{O}_5)$ was 0.042 ± 0.026 on
 649 average with a median of 0.035, ranging from 0.0045 to 0.12 (Figure 13). These results are

650 comparable to that previously determined in the North of China using various different
 651 methods (Wang et al., 2017b; Wang et al., 2018b; Wang et al., 2017d; Wang et al., 2017e; Xia et
 652 al., 2019; Yu et al., 2020a). The k_{wall} of N_2O_5 corresponding to valid $\gamma(\text{N}_2\text{O}_5)$ measurements
 653 was rather stable at an average of $0.0021 \pm 0.0007 \text{ s}^{-1}$, which was consistent with the values
 654 determined at similar RH levels in the laboratory tests. It somehow reflected the robustness of
 655 the status of the flow tube system and the derived results.

656 In the current system, the N_2O_5 concentrations measured at both entrance and exit of the
 657 flow tube are sensitive to the NO fluctuations within the timescale of one sampling mode,
 658 which can induce large uncertainty on calculating $\gamma(\text{N}_2\text{O}_5)$. With our stringent criteria of data
 659 screening, the cases of drastic NO fluctuations were excluded from the analysis. Hence, the
 660 majority of valid $\gamma(\text{N}_2\text{O}_5)$ for this campaign were obtained during the periods of the NO below
 661 2 ppbv, when the clean air mass was dominant at this urban site. Meanwhile, the Sa
 662 concentration within clean episodes were also lower than other periods, with an average of
 663 $159 \mu\text{m}^2 \text{ cm}^{-3}$. The derived $k_{\text{N}_2\text{O}_5}$ ranged from 2.1×10^{-5} to $1.6 \times 10^{-3} \text{ s}^{-1}$ well above the
 664 detection limit, which demonstrated the robustness of results even subject to low ambient Sa
 665 conditions. In order to improve the applicability of $\gamma(\text{N}_2\text{O}_5)$ measurements, future
 666 development is suggested to prioritize the reduction or removal of NO level (at least the
 667 fluctuation of NO) in the sampling system before the entrance of flow tube without the cost of
 668 particles transmission efficiency.



669
 670 **Figure 13.** The histogram distribution of measured $\gamma(\text{N}_2\text{O}_5)$ for valid cases.

671 **7 Summary and conclusion**

672 We report a new development of an aerosol flow tube system coupled with detailed box model
673 to derive $\gamma(\text{N}_2\text{O}_5)$ directly on ambient aerosols. The unique feature of this system is that the
674 sequential N_2O_5 measurement at the both ends of flow tube was applied to improve the
675 accuracy in quantifying $\gamma(\text{N}_2\text{O}_5)$, by taking it as a constraint for the box model to reproduce
676 the decay of introduced N_2O_5 gas source in the flow tube. With the consideration of detailed
677 chemistry related to N_2O_5 , the proposed approach was testified to refrain from the interference
678 of side reactions, induced by the additional N_2O_5 generation, NO titration in the flow tube and
679 variations of air masses between successive sampling modes.

680 A series of laboratory tests were performed to characterize factors affecting $\gamma(\text{N}_2\text{O}_5)$
681 derivation and demonstrate its applicability on $(\text{NH}_4)_2\text{SO}_4$ aerosols. The uncertainties
682 associated with instruments used in the system and potential fluctuations of various parameters
683 were thoroughly discussed in the uncertainty analysis, and we estimated the overall uncertainty
684 of $\gamma(\text{N}_2\text{O}_5)$ to be 16-43% which is subject to NO, NO_2 , O_3 , meteorological parameters,
685 residence time and $\gamma(\text{N}_2\text{O}_5)$ value itself. The detection limit of $\gamma(\text{N}_2\text{O}_5)$ was quantified to be
686 0.0016 at the aerosol surface concentration (S_a) of $200 \mu\text{m}^2 \text{cm}^{-3}$. We deployed this system for
687 field observations of $\gamma(\text{N}_2\text{O}_5)$ at an urban site in Beijing, where strong anthropogenic emission
688 and frequent switch of air mass were encountered. The obtained $\gamma(\text{N}_2\text{O}_5)$ was in comparable
689 level to previously reported values in northern China and demonstrated the robustness of this
690 system during low NO episodes. Further investigations on N_2O_5 heterogeneous chemistry for
691 both laboratory-generated and ambient particles are also available by the introduced approach.
692

693 **Appendix A: Measured VOCs used to calculate NO₃ reactivity in the box model method**

694 A total of 59 kinds of VOCs were measured by GC-FID-MS in this work, half of which
 695 had known rate constants that can be used to parameterize the reaction of NO₃ with VOCs
 696 (mainly compose of alkenes and aromatics) in $\gamma(\text{N}_2\text{O}_5)$ retrieval by box model method (see
 697 also section 3). Their rate constants were obtained from MCM331 or IUPAC and the values at
 698 298K are listed in Table A1.

699 **Table A1.** VOCs used to calculate NO₃ reactivity (k_{NO_3}) in the box model method

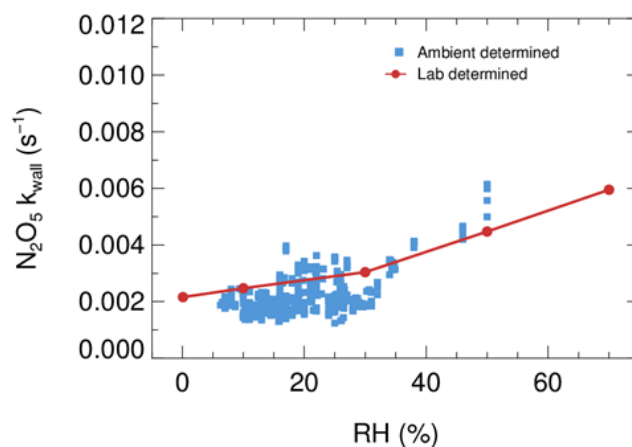
Species	$k_{\text{NO}_3}(298 \text{ K})$	Species	$k_{\text{NO}_3}(298 \text{ K})$
METHANE	1D-18 ^b	TRANS-2-PENTENE	3.70D-13 ^a
ETHANE	1D-17 ^b	1-HEXENE	1.20D-14 ^a
PROPANE	7D-17 ^b	1-3 BUTADIENE	1.03D-13 ^a
N-BUTANE	4.6D-17 ^b	ISOPRENE	7.0D-13 ^b
I-BUTANE	1.1D-16 ^b	STYRENE	1.50D-12 ^a
ETHYLENE	2.1D-16 ^b	ETHYNE	1D-16 ^b
PROPYLENE	9.5D-15 ^b	BENZENE	3D-17 ^b
1-BUTENE	1.3D-14 ^b	TOLUENE	7.8D-17 ^b
CIS-2-BUTENE	3.50D-13 ^a	O-XYLENE	4.10D-16 ^a
TRANS-2-BUTENE	3.90D-13 ^a	M-XYLENE	2.60D-16 ^a
I-BUTENE	3.4D-13 ^b	P-XYLENE	5.00D-16 ^a
1-PENTENE	1.20D-14 ^a	ETHYL BENZENE	1.20D-16 ^a
CIS-2-PENTENE	3.70D-13 ^a	N-PROPYL BENZENE	1.40D-16 ^a

700 Note: a. MCM; b. IUPAC

701

702

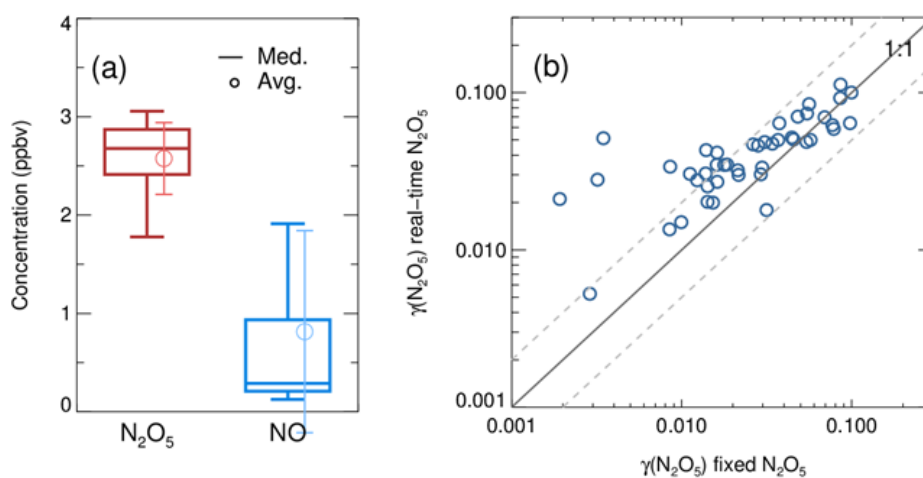
703 **Appendix B: Evaluations of box model method by ambient data.**



704

705 **Figure B1.** The derived dependence of N_2O_5 wall loss on RH at laboratory condition (red
706 dots) and field measurement (blue square)

707



708

709 **Figure B2.** (a) the box whisker of N_2O_5 source and NO measured before the entrance; (b)
710 the inter-comparison of derived N_2O_5 uptake coefficient by using a fixed initial N_2O_5 and a
711 dynamic measured N_2O_5 at the flow tube entrance in the iterative box model.

712

713

714

715 **Code/Data availability.** The datasets used in this study are available from the corresponding
716 author upon request (wanghch27@mail.sysu.edu.cn; k.lu@pku.edu.cn).

717

718 **Author contributions.** K.D.L. and H.C.W. designed the study. X.R.C and H.C.W. analyzed
719 the data and wrote the paper with input from K.D.L.

720

721 **Competing interests.** The authors declare that they have no conflicts of interest.

722

723 **Acknowledgments.** This project is supported by the National Natural Science Foundation of
724 China (21976006, 42175111); the Beijing Municipal Natural Science Foundation for
725 Distinguished Young Scholars (JQ19031); National State Environmental Protection Key
726 Laboratory of Formation and Prevention of Urban Air Pollution Complex (CX2020080578);
727 the special fund of the State Key Joint Laboratory of Environment Simulation and Pollution
728 Control (21K02ESPCP); the National Research Program for Key Issue in Air Pollution
729 Control (DQGG0103-01, 2019YFC0214800). Thanks for the data contributed by field
730 campaign team.

731

732 **References**

733 Ahern, A. T., Goldberger, L., Jahl, L., Thornton, J., and Sullivan, R. C.: Production of N₂O₅ and ClNO₂ through
734 Nocturnal Processing of Biomass-Burning Aerosol, *Environmental Science & Technology*, 52, 550-559,
735 10.1021/acs.est.7b04386, 2018.

736 Anttila, T., Kiendler-Scharr, A., Tillmann, R., and Mentel, T. F.: On the reactive uptake of gaseous compounds
737 by organic-coated aqueous aerosols: Theoretical analysis and application to the heterogeneous hydrolysis of
738 N₂O₅, *J. Phys. Chem. A*, 110, 10435-10443, 10.1021/jp062403c, 2006.

739 Baasandorj, M., Hoch, S. W., Bares, R., Lin, J. C., Brown, S. S., Millet, D. B., Martin, R., Kelly, K., Zarzana, K.
740 J., Whiteman, C. D., Dube, W. P., Tonnesen, G., Jaramillo, I. C., and Sohl, J.: Coupling between Chemical and
741 Meteorological Processes under Persistent Cold-Air Pool Conditions: Evolution of Wintertime PM_{2.5} Pollution
742 Events and N₂O₅ Observations in Utah's Salt Lake Valley, *Environmental Science & Technology*, 51, 5941-5950,
743 10.1021/acs.est.6b06603, 2017.

744 Badger, C. L., Griffiths, P. T., George, I., Abbatt, J. P. D., and Cox, R. A.: Reactive uptake of N₂O₅ by aerosol
745 particles containing mixtures of humic acid and ammonium sulfate, *J. Phys. Chem. A*, 110, 6986-6994,
746 10.1021/jp0562678, 2006.

747 Bertram, A. K., Martin, S. T., Hanna, S. J., Smith, M. L., Bodsworth, A., Chen, Q., Kuwata, M., Liu, A., You, Y.,
748 and Zorn, S. R.: Predicting the relative humidities of liquid-liquid phase separation, efflorescence, and
749 deliquescence of mixed particles of ammonium sulfate, organic material, and water using the organic-to-sulfate
750 mass ratio of the particle and the oxygen-to-carbon elemental ratio of the organic component, *Atmos. Chem.*
751 *Phys.*, 11, 10995-11006, 10.5194/acp-11-10995-2011, 2011.

752 Bertram, T., and Thornton, J.: Toward a general parameterization of N_2O_5 reactivity on aqueous particles: the
753 competing effects of particle liquid water, nitrate and chloride, *Atmos. Chem. Phys.*, 9, 8351-8363, 2009a.

754 Bertram, T. H., and Thornton, J. A.: Toward a general parameterization of N_2O_5 reactivity on aqueous particles:
755 the competing effects of particle liquid water, nitrate and chloride, *Atmos. Chem. Phys.*, 9, 8351-8363,
756 10.5194/acp-9-8351-2009, 2009b.

757 Bertram, T. H., Thornton, J. A., and Riedel, T. P.: An experimental technique for the direct measurement of N_2O_5
758 reactivity on ambient particles, *Atmospheric Measurement Techniques*, 2, 231-242, 10.5194/amt-2-231-2009,
759 2009a.

760 Bertram, T. H., Thornton, J. A., Riedel, T. P., Middlebrook, A. M., Bahreini, R., Bates, T. S., Quinn, P. K., and
761 Coffman, D. J.: Direct observations of N_2O_5 reactivity on ambient aerosol particles, *Geophys. Res. Lett.*, 36,
762 10.1029/2009gl040248, 2009b.

763 Brown, S., Stark, H., Ciciora, S., McLaughlin, R., and Ravishankara, A. R.: Simultaneous in situ Detection of
764 Atmospheric NO_3 and N_2O_5 via Cavity Ring-down Spectroscopy, *Rev. Sci. Instrum.*, 73, 3291-3301,
765 10.1063/1.1499214, 2002.

766 Brown, S. S., Ryerson, T. B., Wollny, A. G., Brock, C. A., Peltier, R., Sullivan, A. P., Weber, R. J., Dube, W. P.,
767 Trainer, M., Meagher, J. F., Fehsenfeld, F. C., and Ravishankara, A. R.: Variability in nocturnal nitrogen oxide
768 processing and its role in regional air quality, *Science*, 311, 67-70, 10.1126/science.1120120, 2006.

769 Brown, S. S., Dube, W. P., Fuchs, H., Ryerson, T. B., Wollny, A. G., Brock, C. A., Bahreini, R., Middlebrook, A.
770 M., Neuman, J. A., Atlas, E., Roberts, J. M., Osthoff, H. D., Trainer, M., Fehsenfeld, F. C., and Ravishankara, A.
771 R.: Reactive uptake coefficients for N_2O_5 determined from aircraft measurements during the Second Texas Air
772 Quality Study: Comparison to current model parameterizations, *J. Geophys. Res.- Atmos.*, 114, D00F10(01-16),
773 Artn D00f10
774 10.1029/2008jd011679, 2009.

775 Brown, S. S., and Stutz, J.: Nighttime radical observations and chemistry, *Chem. Soc. Rev.*, 41, 6405-6447,
776 10.1039/c2cs35181a, 2012.

777 Brown, S. S., Dubé, W. P., Tham, Y. J., Zha, Q., Xue, L., Poon, S., Wang, Z., Blake, D. R., Tsui, W., Parrish, D.
778 D., and Wang, T.: Nighttime chemistry at a high altitude site above Hong Kong, *J. Geophys. Res.: Atmos.*, 121,
779 2457-2475, 10.1002/2015jd024566, 2016.

780 Chang, W. L., Bhave, P. V., Brown, S. S., Riemer, N., Stutz, J., and Dabdub, D.: Heterogeneous atmospheric
781 chemistry, ambient measurements, and model calculations of N_2O_5 : A review, *Aerosol Sci. Technol.*, 45, 665-
782 695, 2011.

783 Chen, X., Wang, H., Lu, K., Li, C., Zhai, T., Tan, Z., Ma, X., Yang, X., Liu, Y., Chen, S., Dong, H., Li, X., Wu,
784 Z., Hu, M., Zeng, L., and Zhang, Y.: Field Determination of Nitrate Formation Pathway in Winter Beijing,
785 *Environmental Science & Technology*, 54, 9243-9253, 10.1021/acs.est.0c00972, 2020.

786 Chen, X., Wang, H., and Lu, K.: Interpretation of $\text{NO}_3\text{-N}_2\text{O}_5$ observation via steady state in high aerosol air
787 mass: The impact of equilibrium coefficient in ambient conditions, *Atmospheric Chemistry and Physics*
788 *Discussions*, 1-14, 2021.

789 Cosman, L. M., Knopf, D. A., and Bertram, A. K.: N_2O_5 reactive uptake on aqueous sulfuric acid solutions

790 coated with branched and straight-chain insoluble organic surfactants, *J. Phys. Chem. A*, 112, 2386-2396,
791 10.1021/jp710685r, 2008.

792 Danckwerts, P. V.: Continuous flow systems: distribution of residence times, *Chem. Eng. Sci.*, 2, 1-13, 1953.

793 Davis, J. M., Bhave, P. V., and Foley, K. M.: Parameterization of N₂O₅ reaction probabilities on the surface of
794 particles containing ammonium, sulfate, and nitrate, *Atmos. Chem. Phys.*, 8, 5295-5311, 10.5194/acp-8-5295-
795 2008, 2008.

796 Dentener, F. J., and Crutzen, P. J.: Reaction Of N₂O₅ On Tropospheric Aerosols - Impact On The Global
797 Distributions Of NO_x, O₃, And OH, *Journal of Geophysical Research Atmospheres*, 98, 7149-7163, 1993.

798 Escoreia, E. N., Sjostedt, S. J., and Abbatt, J. P. D.: Kinetics of N₂O₅ Hydrolysis on Secondary Organic Aerosol
799 and Mixed Ammonium Bisulfate-Secondary Organic Aerosol Particles, *J. Phys. Chem. A*, 114, 13113-13121,
800 10.1021/jp107721v, 2010.

801 Evans, M., and Jacob, D. J.: Impact of new laboratory studies of N₂O₅ hydrolysis on global model budgets of
802 tropospheric nitrogen oxides, ozone, and OH, *Geophys. Res. Lett.*, 32, 2005.

803 Folkers, M., Mentel, T. F., and Wahner, A.: Influence of an organic coating on the reactivity of aqueous aerosols
804 probed by the heterogeneous hydrolysis of N₂O₅, *Geophys. Res. Lett.*, 30, Artn 1644
805 10.1029/2003gl017168, 2003.

806 Fried, A., Henry, B. E., Calvert, J. G., and Mozurkewich, M.: THE REACTION PROBABILITY OF N₂O₅ WITH
807 SULFURIC-ACID AEROSOLS AT STRATOSPHERIC TEMPERATURES AND COMPOSITIONS, *J.*
808 *Geophys. Res.- Atmos.*, 99, 3517-3532, 10.1029/93jd01907, 1994.

809 Fu, X., Wang, T., Gao, J., Wang, P., Liu, Y., Wang, S., Zhao, B., and Xue, L.: Persistent Heavy Winter Nitrate
810 Pollution Driven by Increased Photochemical Oxidants in Northern China, *Environ. Sci. Technol.*, 54, 3881-3889,
811 10.1021/acs.est.9b07248, 2020.

812 Fuchs, N. A., and Sutugin, A. G.: Highly Dispersed Aerosol, Halsted Press, 1970.

813 Gaston, C. J., Thornton, J. A., and Ng, N. L.: Reactive uptake of N₂O₅ to internally mixed inorganic and organic
814 particles: the role of organic carbon oxidation state and inferred organic phase separations, *Atmos. Chem. Phys.*,
815 14, 5693-5707, 10.5194/acp-14-5693-2014, 2014.

816 Gaston, C. J., and Thornton, J. A.: Reacto-Diffusive Length of N₂O₅ in Aqueous Sulfate- and Chloride-
817 Containing Aerosol Particles, *J. Phys. Chem. A*, 120, 1039-1045, 10.1021/acs.jpca.5b11914, 2016.

818 Griffiths, P. T., Badger, C. L., Cox, R. A., Folkers, M., Henk, H. H., and Mentel, T. F.: Reactive Uptake of N₂O₅
819 by Aerosols Containing Dicarboxylic Acids. Effect of Particle Phase, Composition, and Nitrate Content, *J. Phys.*
820 *Chem. A*, 113, 5082-5090, 10.1021/jp8096814, 2009.

821 Gross, S., Iannone, R., Xiao, S., and Bertram, A. K.: Reactive uptake studies of NO₃ and N₂O₅ on alkenoic acid,
822 alkanolate, and polyalcohol substrates to probe nighttime aerosol chemistry, *PCCP*, 11, 7792-7803,
823 10.1039/b904741g, 2009.

824 Hallquist, M., Stewart, D. J., Baker, J., and Cox, R. A.: Hydrolysis of N₂O₅ on submicron sulfuric acid aerosols,
825 *J. Phys. Chem. A*, 104, 3984-3990, 10.1021/jp9939625, 2000.

826 Hallquist, M., Stewart, D. J., Stephenson, S. K., and Anthony Cox, R.: Hydrolysis of N₂O₅ on sub-micron sulfate
827 aerosols, *PCCP*, 5, 3453, 10.1039/b301827j, 2003.

828 Hu, J. H., and Abbatt, J. P. D.: Reaction probabilities for N₂O₅ hydrolysis on sulfuric acid and ammonium sulfate
829 aerosols at room temperature, *J. Phys. Chem. A*, 101, 871-878, DOI 10.1021/jp9627436, 1997.

830 Huang, Y., Coggon, M., Zhao, R., Lignell, H., Bauer, M., Flagan, R., and Seinfeld, J.: The Caltech Photooxidation
831 Flow Tube reactor: Design, fluid dynamics and characterization, *Atmospheric Measurement Techniques*, 10, 839-
832 867, 10.5194/amt-10-839-2017, 2017.

833 Kane, S. M., Caloz, F., and Leu, M. T.: Heterogeneous uptake of gaseous N_2O_5 by $(NH_4)_2SO_4$, NH_4HSO_4 , and
834 H_2SO_4 aerosols, *J. Phys. Chem. A*, 105, 6465-6470, 10.1021/jp010490x, 2001.

835 Karagulian, F., Santschi, C., and Rossi, M.: The heterogeneous chemical kinetics of N_2O_5 on $CaCO_3$ and
836 other atmospheric mineral dust surrogates, *Atmos. Chem. Phys.*, 6, 1373-1388, 2006.

837 Lambe, A., Ahern, A., Williams, L., Slowik, J., Wong, J., Abbatt, J., Brune, W., Ng, N., Wright, J., and Croasdale,
838 D.: Characterization of aerosol photooxidation flow reactors: heterogeneous oxidation, secondary organic aerosol
839 formation and cloud condensation nuclei activity measurements, *Atmospheric Measurement Techniques*, 4, 445-
840 461, 2011.

841 Li, C. M., Wang, H. C., Chen, X. R., Zhai, T. Y., Chen, S. Y., Li, X., Zeng, L. M., and Lu, K. D.: Thermal
842 dissociation cavity-enhanced absorption spectrometer for measuring NO_2 , RO_2NO_2 , and $RONO_2$ in the
843 atmosphere, *Atmospheric Measurement Techniques*, 14, 4033-4051, 10.5194/amt-14-4033-2021, 2021.

844 Li, Q., Zhang, L., Wang, T., Tham, Y. J., Ahmadov, R., Xue, L., Zhang, Q., and Zheng, J.: Impacts of
845 heterogeneous uptake of dinitrogen pentoxide and chlorine activation on ozone and reactive nitrogen partitioning:
846 improvement and application of the WRF-Chem model in southern China, *Atmos. Chem. Phys.*, 16, 14875-14890,
847 10.5194/acp-16-14875-2016, 2016.

848 Liu, X., Gu, J., Li, Y., Cheng, Y., Qu, Y., Han, T., Wang, J., Tian, H., Chen, J., and Zhang, Y.: Increase of aerosol
849 scattering by hygroscopic growth: Observation, modeling, and implications on visibility, *Atmos. Res.*, 132, 91-
850 101, 2013.

851 Lowe, D., Archer-Nicholls, S., Morgan, W., Allan, J., Utembe, S., Ouyang, B., Aruffo, E., Le Breton, M., Zaveri,
852 R. A., and Di Carlo, P.: WRF-Chem model predictions of the regional impacts of N_2O_5 heterogeneous processes
853 on night-time chemistry over north-western Europe, *Atmos. Chem. Phys.*, 15, 1385-1409, 2015.

854 Macintyre, H., and Evans, M.: Sensitivity of a global model to the uptake of N_2O_5 by tropospheric aerosol,
855 *Atmos. Chem. Phys.*, 10, 7409-7414, 2010.

856 Martin, S. T.: Phase transitions of aqueous atmospheric particles, *Chem. Rev.*, 100, 3403-3454, 2000.

857 McDuffie, E. E., Fibiger, D. L., Dubé, W. P., Lopez-Hilfiker, F., Lee, B. H., Thornton, J. A., Shah, V., Jaeglé, L.,
858 Guo, H., Weber, R. J., Michael Reeves, J., Weinheimer, A. J., Schroder, J. C., Campuzano-Jost, P., Jimenez, J. L.,
859 Dibb, J. E., Veres, P., Ebben, C., Sparks, T. L., Wooldridge, P. J., Cohen, R. C., Hornbrook, R. S., Apel, E. C.,
860 Campos, T., Hall, S. R., Ullmann, K., and Brown, S. S.: Heterogeneous N_2O_5 Uptake During Winter: Aircraft
861 Measurements During the 2015 WINTER Campaign and Critical Evaluation of Current Parameterizations, *J.*
862 *Geophys. Res.: Atmos.*, 123, 4345-4372, 10.1002/2018jd028336, 2018.

863 McDuffie, E. E., Womack, C. C., Fibiger, D. L., Dube, W. P., Franchin, A., Middlebrook, A. M., Goldberger, L.,
864 Lee, B. H., Thornton, J. A., Moravek, A., Murphy, J. G., Baasandorj, M., and Brown, S. S.: On the contribution
865 of nocturnal heterogeneous reactive nitrogen chemistry to particulate matter formation during wintertime
866 pollution events in Northern Utah, *Atmos. Chem. Phys.*, 19, 9287-9308, 10.5194/acp-19-9287-2019, 2019.

867 McNeill, V. F., Patterson, J., Wolfe, G. M., and Thornton, J. A.: The effect of varying levels of surfactant on the
868 reactive uptake of N_2O_5 to aqueous aerosol, *Atmos. Chem. Phys.*, 6, 1635-1644, 10.5194/acp-6-1635-2006, 2006.

869 Mentel, T. F., Sohn, M., and Wahner, A.: Nitrate effect in the heterogeneous hydrolysis of dinitrogen pentoxide
870 on aqueous aerosols, *PCCP*, 1, 5451-5457, 10.1039/a905338g, 1999.

871 Mielke, L. H., Stutz, J., Tsai, C., Hurlock, S. C., Roberts, J. M., Veres, P. R., Froyd, K. D., Hayes, P. L., Cubison,
872 M. J., Jimenez, J. L., Washenfelder, R. A., Young, C. J., Gilman, J. B., de Gouw, J. A., Flynn, J. H., Grossberg,
873 N., Lefer, B. L., Liu, J., Weber, R. J., and Osthoff, H. D.: Heterogeneous formation of nitryl chloride and its role
874 as a nocturnal NO_x reservoir species during CalNex-LA 2010, *J. Geophys. Res.: Atmos.*, 118, 6038-6106, 2013,
875 10.1002/jgrd.50783, 2013.

876 Mitroo, D., Gill, T. E., Haas, S., Pratt, K. A., and Gaston, C. J.: ClNO₂ Production from N₂O₅ Uptake on Saline
877 Playa Dusts: New Insights into Potential Inland Sources of ClNO₂, *Environmental Science & Technology*, 53,
878 7442-7452, 10.1021/acs.est.9b01112, 2019.

879 Mozurkewich, M., and Calvert, J. G.: REACTION PROBABILITY OF N₂O₅ ON AQUEOUS AEROSOLS, *J.*
880 *Geophys. Res.- Atmos.*, 93, 15889-15896, 10.1029/JD093iD12p15889, 1988.

881 Murray, L. T., Fiore, A. M., Shindell, D. T., Naik, V., and Horowitz, L. W.: Large uncertainties in global hydroxyl
882 projections tied to fate of reactive nitrogen and carbon, *Proceedings of the National Academy of Sciences*, 118,
883 2021.

884 Osthoff, H. D., Roberts, J. M., Ravishankara, A. R., Williams, E. J., Lerner, B. M., Sommariva, R., Bates, T. S.,
885 Coffman, D., Quinn, P. K., Dibb, J. E., Stark, H., Burkholder, J. B., Talukdar, R. K., Meagher, J., Fehsenfeld, F.
886 C., and Brown, S. S.: High levels of nitryl chloride in the polluted subtropical marine boundary layer, *Nat.*
887 *Geosci.*, 1, 324-328, 10.1038/ngeo177, 2008.

888 Phillips, G. J., Thieser, J., Tang, M., Sobanski, N., Schuster, G., Fachinger, J., Drewnick, F., Borrmann, S.,
889 Bingemer, H., Lelieveld, J., and Crowley, J. N.: Estimating N₂O₅ uptake coefficients using ambient measurements
890 of NO₃, N₂O₅, ClNO₂ and particle-phase nitrate, *Atmos. Chem. Phys.*, 16, 13231-13249, 10.5194/acp-16-13231-
891 2016, 2016.

892 Platt, U. F., Winer, A. M., Biermann, H. W., Atkinson, R., and Pitts, J. N.: Measurement of nitrate radical
893 concentrations in continental air, *Environmental Science & Technology*, 18, 365-369, 10.1021/es00123a015,
894 1984.

895 Prabhakar, G., Parworth, C. L., Zhang, X. L., Kim, H., Young, D. E., Beyersdorf, A. J., Ziemba, L. D., Nowak,
896 J. B., Bertram, T. H., Faloona, I. C., Zhang, Q., and Cappa, C. D.: Observational assessment of the role of
897 nocturnal residual-layer chemistry in determining daytime surface particulate nitrate concentrations, *Atmos.*
898 *Chem. Phys.*, 17, 14747-14770, 10.5194/acp-17-14747-2017, 2017.

899 Riedel, T. P., Bertram, T. H., Crisp, T. A., Williams, E. J., Lerner, B. M., Vlasenko, A., Li, S. M., Gilman, J., de
900 Gouw, J., Bon, D. M., Wagner, N. L., Brown, S. S., and Thornton, J. A.: Nitryl Chloride and Molecular Chlorine
901 in the Coastal Marine Boundary Layer, *Environmental Science & Technology*, 46, 10463-10470,
902 10.1021/es204632r, 2012a.

903 Riedel, T. P., Bertram, T. H., Ryder, O. S., Liu, S., Day, D. A., Russell, L. M., Gaston, C. J., Prather, K. A., and
904 Thornton, J. A.: Direct N₂O₅ reactivity measurements at a polluted coastal site, *Atmos. Chem. Phys.*, 12, 2959-
905 2968, 10.5194/acp-12-2959-2012, 2012b.

906 Riedel, T. P., Wagner, N. L., Dube, W. P., Middlebrook, A. M., Young, C. J., Ozturk, F., Bahreini, R., VandenBoer,
907 T. C., Wolfe, D. E., Williams, E. J., Roberts, J. M., Brown, S. S., and Thornton, J. A.: Chlorine activation within
908 urban or power plant plumes: Vertically resolved ClNO₂ and Cl₂ measurements from a tall tower in a polluted
909 continental setting, *J. Geophys. Res.- Atmos.*, 118, 8702-8715, 10.1002/jgrd.50637, 2013.

910 Riemer, N., Vogel, H., Vogel, B., Schell, B., Ackermann, I., Kessler, C., and Hass, H.: Impact of the heterogeneous
911 hydrolysis of N₂O₅ on chemistry and nitrate aerosol formation in the lower troposphere under photosmog
912 conditions, *J. Geophys. Res.- Atmos.*, 108, 10.1029/2002jd002436, 2003.

913 Riemer, N., Vogel, H., Vogel, B., Anttila, T., Kiendler-Scharr, A., and Mentel, T. F.: Relative importance of
914 organic coatings for the heterogeneous hydrolysis of N₂O₅ during summer in Europe, *J. Geophys. Res.*, 114,
915 10.1029/2008jd011369, 2009.

916 Royer, H. M., Mitroo, D., Hayes, S. M., Haas, S. M., Pratt, K. A., Blackwelder, P. L., Gill, T. E., and Gaston, C.
917 J.: The Role of Hydrates, Competing Chemical Constituents, and Surface Composition on ClNO₂ Formation,
918 *Environmental Science & Technology*, 55, 2869-2877, 10.1021/acs.est.0c06067, 2021.

919 Sarwar, G., Simon, H., Bhawe, P., and Yarwood, G.: Examining the impact of heterogeneous nitryl chloride
920 production on air quality across the United States, *Atmospheric Chemistry & Physics*, 12, 6455-6473,
921 10.5194/acp-12-6455-2012, 2012.

922 Schweitzer, F., Mirabel, P., and George, C.: Multiphase chemistry of N₂O₅, ClNO₂, and BrNO₂, *The Journal of*
923 *Physical Chemistry A*, 102, 3942-3952, 1998.

924 Tang, M., Telford, P., Pope, F. D., Rkiouak, L., Abraham, N., Archibald, A. T., Braesicke, P., Pyle, J., McGregor,
925 J., and Watson, I.: Heterogeneous reaction of N₂O₅ with airborne TiO₂ particles and its implication for
926 stratospheric particle injection, *Atmos. Chem. Phys.*, 14, 6035-6048, 2014.

927 Tham, Y. J., Wang, Z., Li, Q. Y., Yun, H., Wang, W. H., Wang, X. F., Xue, L. K., Lu, K. D., Ma, N., Bohn, B., Li,
928 X., Kecorius, S., Gross, J., Shao, M., Wiedensohler, A., Zhang, Y. H., and Wang, T.: Significant concentrations
929 of nitryl chloride sustained in the morning: investigations of the causes and impacts on ozone production in a
930 polluted region of northern China, *Atmos. Chem. Phys.*, 16, 14959-14977, 10.5194/acp-16-14959-2016, 2016.

931 Tham, Y. J., Wang, Z., Li, Q. Y., Wang, W. H., Wang, X. F., Lu, K. D., Ma, N., Yan, C., Kecorius, S., Wiedensohler,
932 A., Zhang, Y. H., and Wang, T.: Heterogeneous N₂O₅ uptake coefficient and production yield of ClNO₂ in
933 polluted northern China: roles of aerosol water content and chemical composition, *Atmos. Chem. Phys.*, 18,
934 13155-13171, 10.5194/acp-18-13155-2018, 2018.

935 Thornton, J. A., Braban, C. F., and Abbatt, J. P. D.: N₂O₅ hydrolysis on sub-micron organic aerosols: the effect
936 of relative humidity, particle phase, and particle size, *PCCP*, 5, 4593, 10.1039/b307498f, 2003.

937 Thornton, J. A., and Abbatt, J. P. D.: N₂O₅ reaction on submicron sea salt aerosol: Kinetics, products, and the
938 effect of surface active organics, *J. Phys. Chem. A*, 109, 10004-10012, 10.1021/jp054183t, 2005.

939 Thornton, J. A., Kercher, J. P., Riedel, T. P., Wagner, N. L., Cozic, J., Holloway, J. S., Dube, W. P., Wolfe, G. M.,
940 Quinn, P. K., Middlebrook, A. M., Alexander, B., and Brown, S. S.: A large atomic chlorine source inferred from
941 mid-continental reactive nitrogen chemistry, *Nature*, 464, 271-274, 10.1038/nature08905, 2010.

942 Van Doren, J. M., Watson, L. R., Davidovits, P., Worsnop, D. R., Zahniser, M. S., and Kolb, C. E.: Temperature
943 dependence of the uptake coefficients of nitric acid, hydrochloric acid and nitrogen oxide (N₂O₅) by water
944 droplets, *J. Phys. Chem.*, 94, 3265-3269, 1990.

945 Wagner, N. L., Riedel, T. P., Young, C. J., Bahreini, R., Brock, C. A., Dubé, W. P., Kim, S., Middlebrook, A. M.,
946 Öztürk, F., Roberts, J. M., Russo, R., Sive, B., Swarthout, R., Thornton, J. A., VandenBoer, T. C., Zhou, Y., and
947 Brown, S. S.: N₂O₅ uptake coefficients and nocturnal NO₂ removal rates determined from ambient wintertime
948 measurements, *J. Geophys. Res.: Atmos.*, 118, 9331-9350, 10.1002/jgrd.50653, 2013.

949 Wahner, A., Mentel, T. F., Sohn, M., and Stier, J.: Heterogeneous reaction of N₂O₅ on sodium nitrate aerosol, *J.*
950 *Geophys. Res.: Atmos.*, 103, 31103-31112, 10.1029/1998jd100022, 1998.

951 Wang, H., Chen, J., and Lu, K.: Development of a portable cavity-enhanced absorption spectrometer for the
952 measurement of ambient NO₃ and
953 N₂O₅: experimental setup, lab characterizations, and field
954 applications in a polluted urban environment, *Atmospheric Measurement Techniques*, 10, 1465-1479,
955 10.5194/amt-10-1465-2017, 2017a.

956 Wang, H., Lu, K., Chen, X., Zhu, Q., Chen, Q., Guo, S., Jiang, M., Li, X., Shang, D., Tan, Z., Wu, Y., Wu, Z.,
957 Zou, Q., Zheng, Y., Zeng, L., Zhu, T., Hu, M., and Zhang, Y.: High N₂O₅ Concentrations Observed in Urban
958 Beijing: Implications of a Large Nitrate Formation Pathway, *Environ Sci Tech Let*, 4, 416-420,
959 10.1021/acs.estlett.7b00341, 2017b.

960 Wang, H., Chen, X., Lu, K., Tan, Z., Ma, X., Wu, Z., Li, X., Liu, Y., Shang, D., Wu, Y., Zeng, L., Hu, M., Schmitt,
961 S., Kiendler-Scharr, A., Wahner, A., and Zhang, Y.: Wintertime N₂O₅ uptake coefficients over the North China

962 Plain, *Science Bulletin*, 65, 765-774, <https://doi.org/10.1016/j.scib.2020.02.006>, 2020a.

963 Wang, H. C., Lu, K. D., Chen, X. R., Zhu, Q. D., Chen, Q., Guo, S., Jiang, M. Q., Li, X., Shang, D. J., Tan, Z. F.,
964 Wu, Y. S., Wu, Z. J., Zou, Q., Zheng, Y., Zeng, L. M., Zhu, T., Hu, M., and Zhang, Y. H.: High N₂O₅
965 Concentrations Observed in Urban Beijing: Implications of a Large Nitrate Formation Pathway, *Environ Sci Tech*
966 *Let*, 4, 416-420, 10.1021/acs.estlett.7b00341, 2017c.

967 Wang, H. C., Lu, K. D., Chen, X. R., Zhu, Q. D., Wu, Z. J., Wu, Y. S., and Sun, K.: Fast particulate nitrate
968 formation via N₂O₅ uptake aloft in winter in Beijing, *Atmos. Chem. Phys.*, 18, 10483-10495, 10.5194/acp-18-
969 10483-2018, 2018a.

970 Wang, H. C., Lu, K. D., Guo, S., Wu, Z. J., Shang, D. J., Tan, Z. F., Wang, Y. J., Le Breton, M., Lou, S. R., Tang,
971 M. J., Wu, Y. S., Zhu, W. F., Zheng, J., Zeng, L. M., Hallquist, M., Hu, M., and Zhang, Y. H.: Efficient N₂O₅
972 uptake and NO₃ oxidation in the outflow of urban Beijing, *Atmos. Chem. Phys.*, 18, 9705-9721, 10.5194/acp-
973 18-9705-2018, 2018b.

974 Wang, H. C., Chen, X. R., Lu, K. D., Hu, R. Z., Li, Z. Y., Wang, H. L., Ma, X. F., Yang, X. P., Chen, S. Y., Dong,
975 H. B., Liu, Y., Fang, X., Zeng, L. M., Hu, M., and Zhang, Y. H.: NO₃ and N₂O₅ chemistry at a suburban site
976 during the EXPLORE-YRD campaign in 2018, *Atmos. Environ.*, 224, ARTN 117180
977 10.1016/j.atmosenv.2019.117180, 2020b.

978 Wang, H. C., Peng, C., Wang, X., Lou, S. R., Lu, K. D., Gan, G. C., Jia, X. H., Chen, X. R., Chen, J., Wang, H.
979 L., Fan, S. J., Wang, X. M., and Tang, M. J.: N₂O₅ uptake onto saline mineral dust: a potential missing source of
980 tropospheric ClNO₂ in inland China, *Atmos. Chem. Phys.*, 22, 1845-1859, 10.5194/acp-22-1845-2022, 2022.

981 Wang, W., Wang, Z., Yu, C., Xia, M., Peng, X., Zhou, Y., Yue, D., Ou, Y., and Wang, T.: An in situ flow tube
982 system for direct measurement of N₂O₅ heterogeneous uptake coefficients in polluted environments,
983 *Atmospheric Measurement Techniques*, 11, 5643-5655, 10.5194/amt-11-5643-2018, 2018c.

984 Wang, X., Wang, H., Xue, L., Wang, T., Wang, L., Gu, R., Wang, W., Tham, Y. J., Wang, Z., Yang, L., Chen, J.,
985 and Wang, W.: Observations of N₂O₅ and ClNO₂ at a polluted urban surface site in North China: High N₂O₅
986 uptake coefficients and low ClNO₂ product yields, *Atmos. Environ.*, 156, 125-134,
987 10.1016/j.atmosenv.2017.02.035, 2017d.

988 Wang, Y. L., Song, W., Yang, W., Sun, X. C., Tong, Y. D., Wang, X. M., Liu, C. Q., Bai, Z. P., and Liu, X. Y.:
989 Influences of atmospheric pollution on the contributions of major oxidation pathways to PM_{2.5} nitrate formation
990 in Beijing, *J. Geophys. Res.: Atmos.*, 124, 4174-4185, 2019.

991 Wang, Z., Wang, W., Tham, Y. J., Li, Q., Wang, H., Wen, L., Wang, X., and Wang, T.: Fast heterogeneous N₂O₅
992 uptake and ClNO₂ production in power plant and industrial plumes observed in the nocturnal residual layer over
993 the North China Plain, *Atmos. Chem. Phys.*, 17, 12361-12378, 10.5194/acp-17-12361-2017, 2017e.

994 Wang, Z., Wang, W. H., Tham, Y. J., Li, Q. Y., Wang, H., Wen, L., Wang, X. F., and Wang, T.: Fast heterogeneous
995 N₂O₅ uptake and ClNO₂ production in power plant and industrial plumes observed in the nocturnal residual
996 layer over the North China Plain, *Atmos. Chem. Phys.*, 17, 12361-12378, 10.5194/acp-17-12361-2017, 2017f.

997 Wu, C., Zhang, S., Wang, G., Lv, S., Li, D., Liu, L., Li, J., Liu, S., Du, W., and Meng, J.: Efficient heterogeneous
998 formation of ammonium nitrate on the saline mineral particle surface in the atmosphere of East Asia during dust
999 storm periods, *Environmental Science & Technology*, 54, 15622-15630, 2020.

1000 Xia, M., Wang, W., Wang, Z., Gao, J., Li, H., Liang, Y., Yu, C., Zhang, Y., Wang, P., Zhang, Y., Bi, F., Cheng, X.,
1001 and Tao, W.: Heterogeneous Uptake of N₂O₅ in Sand Dust and Urban Aerosols Observed during the Dry Season
1002 in Beijing, *Atmosphere*, 10, 204, 10.3390/atmos10040204, 2019.

1003 Yu, C., Wang, Z., Xia, M., Fu, X., Wang, W., Yee Jun, T., Chen, T., Zheng, P., Li, H., Shan, Y., Wang, X., Xue,
1004 L., Zhou, Y., Yue, D., Ou, Y., Gao, J., Lu, K., Brown, S., Zhang, Y., and Tao, W.: Heterogeneous N₂O₅ reactions

1005 on atmospheric aerosols at four Chinese sites: improving model representation of uptake parameters, *Atmos.*
1006 *Chem. Phys.*, 20, 4367-4378, 10.5194/acp-20-4367-2020, 2020a.
1007 Yu, C., Wang, Z., Xia, M., Fu, X., Wang, W. H., Tham, Y. J., Chen, T. S., Zheng, P. G., Li, H. Y., Shan, Y., Wang,
1008 X. F., Xue, L. K., Zhou, Y., Yue, D. L., Ou, Y. B., Gao, J., Lu, K. D., Brown, S. S., Zhang, Y. H., and Wang, T.:
1009 Heterogeneous N₂O₅ reactions on atmospheric aerosols at four Chinese sites: improving model representation
1010 of uptake parameters, *Atmos. Chem. Phys.*, 20, 4367-4378, 10.5194/acp-20-4367-2020, 2020b.
1011 Yun, H., Wang, T., Wang, W. H., Tham, Y. J., Li, Q. Y., Wang, Z., and Poon, S. C. N.: Nighttime NO_x loss and
1012 ClNO₂ formation in the residual layer of a polluted region: Insights from field measurements and an iterative
1013 box model, *Sci. Total Environ.*, 622, 727-734, 10.1016/j.scitotenv.2017.11.352, 2018.
1014